https://doi.org/10.5194/esurf-2021-104
Preprint. Discussion started: 11 January 2022
© Author(s) 2022. CC BY 4.0 License.

Earth Surface Dynamics Discussions
Open Access

Time-Of-Flight monitoring reveals higher sediment redistribution rates related to burrowing animals than previously assumed

Paulina Grigusova[1], Annegret Larsen[2], Sebastian Achilles[1], Roland Brandl[3], Camilo del Río[4,5], Nina Farwig[6], Diana Kraus[6], Leandro Paulino[7], Patricio Pliscoff[4,8,9], Kirstin Übernickel[10], Jörg Bendix[1]

[1] Laboratory for Climatology and Remote Sensing, Department of Geography, University of Marburg, 35037 Marburg, Germany; paulina.grigusova@staff.uni-marburg.de (P.G.); bendix@geo.uni-marburg.de (J.B.)

[2] Soil Geography and Landscape, Department of Environmental Sciences, Wageningen University & Research, 6700 AA Wageningen, The Netherlands; annegret.larsen@wur.nl

[3] Animal Ecology, Department of Biology, University of Marburg, 35032 Marburg, Germany; brandlr@biologie.uni-marburg.de

[4] Facultad de Historia, Geografía y Ciencia Política, Instituto de Geografía, Pontificia Universidad Católica de Chile, 782-0436 Santiago, Chile; pliscoff@uc.cl; cdelriol@uc.cl

[5] Centro UC Desierto de Atacama, Pontificia Universidad Católica de Chile, 782-0436 Santiago, Chile; cdelriol@uc.cl

[6] Conservation Ecology, Department of Biology, University of Marburg, 35047 Marburg, Germany; diana.kraus@biologie.uni-marburg.de (D.K.); nina.farwig@biologie.uni-marburg.de (N.F.)

[7] Facultad de Agronomía, Universidad de Concepción, 3780000 Chillán, Chile; lpaulino@udec.cl

[8] Facultad de Ciencias Biológicas, Departamento de Ecología, Pontificia Universidad Católica de Chile, 8331150 Santiago, Chile; pliscoff@uc.cl

[9] Center of Applied Ecology and Sustainability (CAPES), Pontificia Universidad Católica de Chile, 8331150 Santiago, Chile; pliscoff@uc.cl

[10] Earth System Dynamics, Department of Geosciences, University of Tübingen, 72076 Tübingen, Germany; kirstin.uebernickel@uni-tuebingen.de

Corresponding author:
Paulina Grigusova
paulina.grigusova@staff.uni-marburg.de

https://doi.org/10.5194/esurf-2021-104
Preprint. Discussion started: 11 January 2022
© Author(s) 2022. CC BY 4.0 License.

Earth Surface Dynamics Discussions

Abstract

Burrowing animals influence surface microtopography and hillslope sediment redistribution, but changes often remain undetected due to a lack of autonomous high resolution field monitoring techniques. In this study we present a new approach to quantify microtopographic variations and surface changes caused by burrowing animals and rainfall-driven erosional processes applied to remote field plots in arid and mediterranean Chile. We compared the mass balance of redistributed sediment within plot areas affected and not affected by burrowing animals, quantified the cumulative sediment redistribution caused by animals and rainfall, and upscaled the results to the hillslope scale. The new instrument showed a very good detection accuracy. The cumulative sediment redistribution within areas affected by burrowing animals was higher (-10.44 cm^3 cm^{-2} $year^{-1}$) in the mediterranean than the arid climate zone (-1.41 cm^3 cm^{-2} $year^{-1}$). Daily sediment redistribution during rainfall within areas affected by burrowing animals were up to 350% / 40% higher in the mediterranean / arid zone compared to the unaffected areas, and much higher than previously reported in studies not based on continuous microtopographic monitoring. Furthermore, 38% of the sediment eroding from the burrows accumulated within the burrow entrance while 62% was incorporated into overall hillslope sediment flux. The cumulative sediment excavation by the animals was 14.62 cm^3 cm^{-2} $year^{-1}$ in the mediterranean and 16.41 cm^3 cm^{-2} $year^{-1}$ in the arid climate zone. Our findings can be implemented into long-term soil erosion models that rely on soil processes but do not yet include animal-induced surface processes on microtopographical scales in their algorithms.

Keywords: Biogeomorphology, bioturbation, sediment transport, burrowing animals, rainfall, Time-of-Flight camera, Chile

https://doi.org/10.5194/esurf-2021-104
Preprint. Discussion started: 11 January 2022
© Author(s) 2022. CC BY 4.0 License.
Earth Surface Dynamics
Discussions
Open Access

Graphical abstract

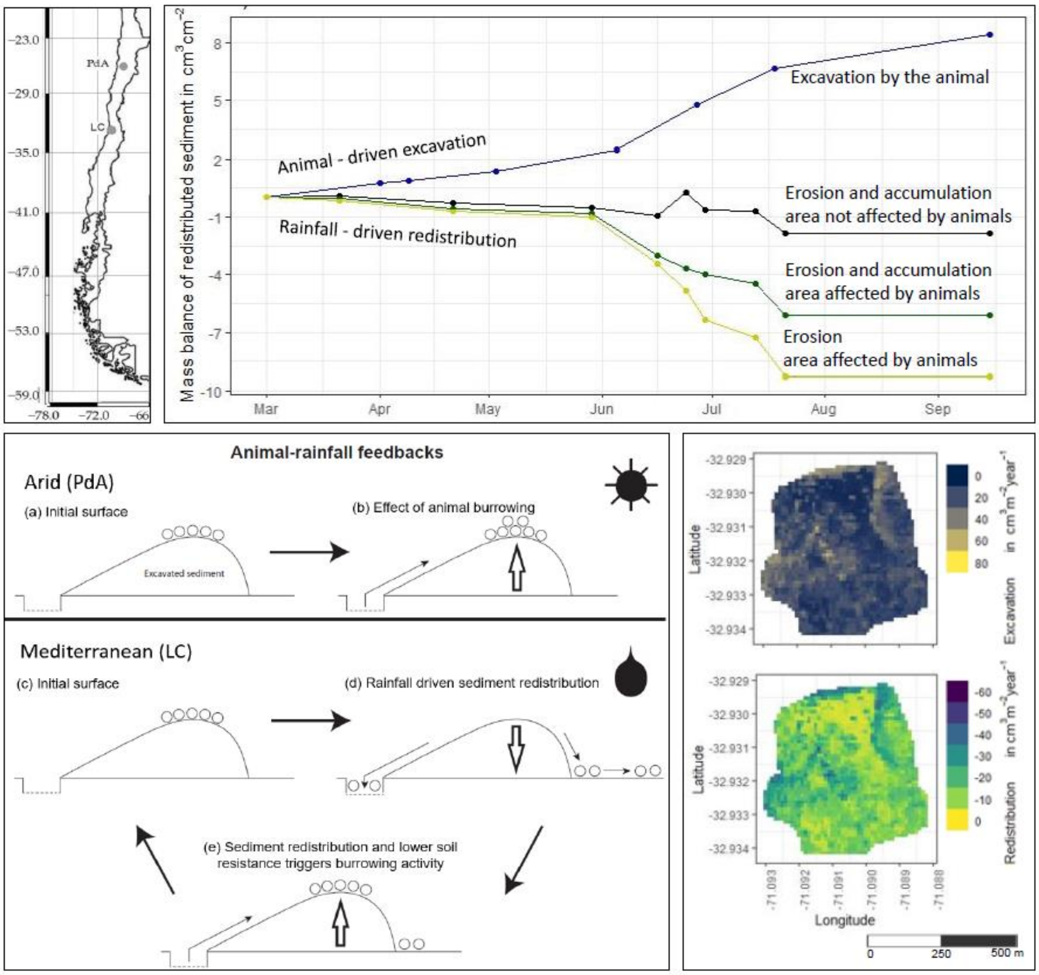

https://doi.org/10.5194/esurf-2021-104
Preprint. Discussion started: 11 January 2022
© Author(s) 2022. CC BY 4.0 License.
Earth Surface Dynamics Discussions

1. Introduction

Animal burrowing activity affects surface microtopography (Reichman and Seabloom, 2002; Kinlaw and Grasmueck, 2012), surface roughness (Yair, 1995; Jones et al., 2010; Hancock and Lowry, 2021) and soil physical properties (Ridd, 1996; Yair, 1995; Hall et al., 1999; Reichman and Seabloom, 2002; Hancock and Lowry, 2021; Coombes, 2016; Larsen et al., 2021). Previous studies estimated both positive as well as negative impacts of burrowing animals on sediment redistribution rates. The results were obtained by applying tests under laboratory conditions using rainfall simulators, conducting several field campaigns weeks to months apart, or by measuring the volume of excavated or eroded sediment in the field using methods such as erosion pins, splash boards, or simple rulers (Imeson and Kwaad, 1976; Reichman and Seabloom, 2002; Wei et al., 2007; Le Hir et al., 2007; Li et al., 2018; Li et al., 2019c; Li et al., 2019b; Voiculescu et al., 2019; Chen et al., 2021; Übernickel et al., 2021b; Li et al., 2019a). Although burrowing animals are generally seen as ecosystem engineers (Gabet et al., 2003; Wilkinson et al., 2009), their role in soil erosion, in general, and for numerical soil erosion models, in particular, is, to date, limited to predictions of the burrow locations and particle mixing at these locations (Black and Montgomery, 1991; Meysman et al., 2003; Yoo et al., 2005; Schiffers et al., 2011). The complex interaction of sediment excavation and accumulation and erosion processes at the burrow and hillslope scales are not yet included in the modelling, as for this, a suitable method capable of measuring all occurred redistribution processes is needed.

The reason for this knowledge gap is that previous studies have not provided data on low magnitude but frequently occurring sediment redistribution due to the specific limitations of their approaches. Field experiments with, for example, rainfall simulators can unveil processes but cannot cover the time-dependant natural dynamics of sediment redistribution. For data samplings that used methods such as erosion pins or splash boards, the sites had to be revisited each time and the data were thus obtained only sporadically (Imeson and Kwaad, 1976; Hazelhoff et al., 1981; Richards and Humphreys, 2010). Similarly, estimations of the excavated sediment volume are currently limited to one-time measurements or studies conducted several months apart (Black and Montgomery, 1991; Hall et al., 1999; Yoo et al., 2005). We expect that non-continuously conducted measurements do not include all frequently occurring excavation and erosion processes. For this, a spatio-temporally high-resolution and continuous monitoring of sediment redistribution is needed.

High-resolution, ground-based imaging sensing techniques might overcome such aforementioned problems. Terrestrial laser scanner systems have shown to be a suitable tool for estimation of sediment redistribution and erosion processes (Nasermoaddeli and Pasche, 2008; Afana et al., 2010; Eltner et al., 2016b; Eltner et al., 2016a; Longoni et al., 2016). However, they are expensive and labour-intensive and, thus, the study sites had to be personally revisited for each measurement. A continuous, autonomous monitoring of many mound areas in parallel is thus not possible. However, Time-of-Flight (ToF) technology offers new possibilities for a high-resolution monitoring of sediment redistribution (Eitel et al., 2011; Hänsel et al., 2016) but a cost-effective field monitoring device is still missing.

In our study, we developed, tested and applied a cost-effective Time-Of-flight camera to autonomously monitor the rainfall-driven and animal-driven sediment redistribution in areas affected by burrowing animals with high temporal (four times a day) and spatial (6 mm) resolution. For this, we equipped several plots in remote study sites of Chile in the arid and mediterranean climate zone. We selected these sites in order to analyse sediment redistribution by burrowing activity of vertebrates under different rainfall regimes and as these sites were particularly shown to be strongly affected by burrowing activity (Grigusova et al., 2021). Then,

https://doi.org/10.5194/esurf-2021-104
Preprint. Discussion started: 11 January 2022
© Author(s) 2022. CC BY 4.0 License.

we quantified the daily sediment redistribution within areas affected and not affected by burrowing animals. We analysed the impacts of animal burrowing activity and rainfall on the sediment redistribution and quantified the volume of sediment which is additionally incorporated to the hillslope sediment flux due to presence of burrows. Finally, we estimated sediment redistribution on a burrow scale and upscaled sediment redistribution rates to the entire hillslopes.

2. Study sites

Our study sites were located in the Chilean Coastal Cordillera in two climate zones (Fig. 1): in the National Park Pan de Azúcar (further as Pan de Azúcar or PdA) and the National Park La Campana (further as La Campana or LC). The Las Lomitas site in PdA is located in the arid climate zone of the Atacama Desert with a precipitation rate of 12 mm $year^{-1}$, and it has a mean annual temperature of 16.8 °C (Übernickel et al., 2021a). Here, the vegetation cover is below 5%, and it is dominated by small desert shrubs, several species of cacti (*Eulychnia breviflora, Copiapoa atacamensis)* and biocrusts (Lehnert et al., 2018). LC is located in the mediterranean climate zone with a precipitation rate of 367 mm $year^{-1}$ and a mean annual temperature of 14.1 °C (Übernickel et al., 2021a). LC is dominated by an evergreen sclerophyllous forest with endemic palm trees, *Jubaea chilensis*. Both research sites have a granitic rock base, and the dominating soil texture is sandy loam (Bernhard et al., 2018). In PdA, the study setup consisted of one north-facing and one south-facing hillslope. The hillslope inclinations were ~20°, and a climate station was located ~15 km from the camera sites. In LC, the setup consisted of two north-facing and one south-facing hillslopes. The hillslope inclinations were ~25°, and a climate station was located ~250 m from the south-facing hillslope (Übernickel et al., 2021a).

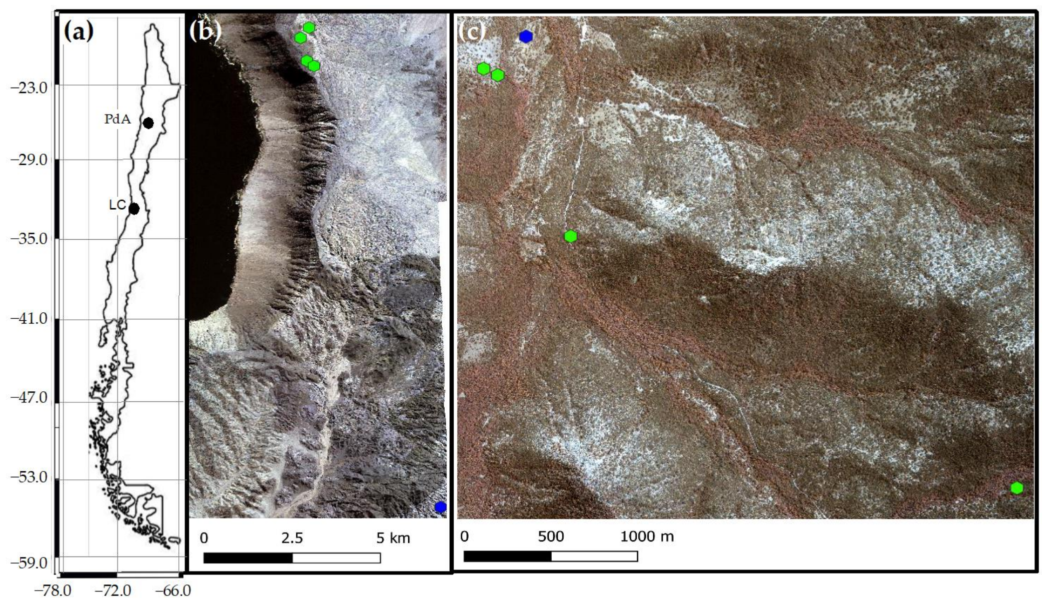

Figure 1. Location of the cameras and climate stations on which this study was based. Black points show the location of the research sites in Chile. The green points represent the camera plots, and the blue points the climate stations: (**a**) Location of study sites in Chile: PdA stands for Pan de Azúcar, LC for La Campana; (**b**)

https://doi.org/10.5194/esurf-2021-104
Preprint. Discussion started: 11 January 2022
© Author(s) 2022. CC BY 4.0 License.
Earth Surface Dynamics Discussions

Study setup in Pan de Azúcar; (**c**) Study setup in LC. The background images in (**b**) and (**c**) are orthophotos created from WorldView-2 data from 19 July 2019. For exact latitude and longitude see Table A2.

3. Methodology

3.1 Time-of-Flight (ToF) principle

A Time-of-Flight-based camera illuminates an object with a light source, usually in a non-visible spectrum, such as near-infrared, for a precise length of time. The here employed cameras were pulse-based, meaning the light pulse was first emitted by the camera, then reflected from the surface, and finally measured by the camera using two temporary windows. The first temporary window measures the incoming reflected light while the light pulse is also still emitting from the camera. The second temporary window measures the incoming reflected light when no pulse is emitting from the camera. The distance from the camera to the object can then be calculated as follows:

$$d = \frac{1}{2} * c * t * \left(\frac{g1}{g1+g2}\right) \quad . \qquad (1)$$

In Eq. (1), d (m) is the distance from the camera to the object, c (m s^{-1}) is the speed of light (299,792,458 m s^{-1}), t (s) is the overall time of the illumination and measurement, g_1 is the ratio of the reflected photons to all photons accumulated in the first window, and g_2 the ratio of the reflected photons to all photons accumulated in the second window (Sarbolandi et al., 2018; Li, 2014).

The sensor in our camera came from Texas Instruments and the data scan contained information on 320 x 240 points. The camera field of view (FOV) and the spatial resolution of the scans depended on the height of the camera above the surface. The distance was calculated for every point, and the object was saved in binary format as a collection of 3D points with *x*-, *y*- and *z*-coordinates. The scans taken by the camera were transformed from the binary format to a point cloud. Each point in the point cloud was assigned to an *x*-, *y*- and *z*-coordinate. The coordinates were distributed within a three-dimensional Euclidian space, with the point at the camera nadir being the point of origin. *x*- and *y*-coordinates describe the distance to the point of origin (m). *z*-coordinate describes the distance (m) from the object to the camera. The lowest point of the scanned surface thus has the highest *z*-coordinate value.

3.2 Data processing

The distortion caused by the hillslope and the camera angle was corrected for each point cloud as follows:

$$z_{cor} = z_{uncor} - \tan(\alpha + \beta) * distance(y_1 - y_i) \quad . \qquad (2)$$

In Eq. (2), z_{cor} is the corrected distance (m) between the camera and surface (m), z_{uncor} is the uncorrected *z*-coordinate (m), α is the tilt angle of the camera (°), β is the surface inclination (°), and y_i is the distance of the point to the point of origin at the camera nadir (m). The most frequent errors were identified and treated as follows. Due to the ambient light reaching the camera sensor, the *z*-coordinate values of some of the points were incorrect (scattering error). To remove this error, a threshold value was calculated for each point cloud:

$$\Omega = mean_{zcor-coordinates} \pm sd_{zcor-coordinates} \quad . \qquad (3)$$

In Eq. (3), Ω is the threshold value, $mean_{zcor\text{-}coordinate}$ is the average value, and $sd_{zcor\text{-}coordinate}$ is the standard deviation of the corrected *z*-coordinates (m). Then all points with a *z*-coordinate above and below this value were deleted. Point clouds with more than 50% of points above the threshold value Ω were also not considered for further processing. A drift error occurred when the *z*-coordinate values of around one-third of the point

https://doi.org/10.5194/esurf-2021-104
Preprint. Discussion started: 11 January 2022
© Author(s) 2022. CC BY 4.0 License.

Earth Surface Dynamics Discussions Open Access EGU

clouds decreased by several centimetres from one point cloud to another. Here, the average *z*-coordinate of ten point clouds before and after the drift were calculated, and the difference was added to *z*-coordinates of the points affected by the drift. The corrected height values were then transformed into a digital surface model (DSM).

3.3 Accuracy of the ToF cameras

The accuracy of the ToF camera was tested under laboratory conditions by recreating similar surface conditions as in the field (sloping surface, covered by sediment). An artificial mound using sediment extracted from a riverbank in central Germany was used, mimicking a mound created by a burrowing animal. During the test, the camera was installed 100 cm above the surface. The camera FOV was 3 m^2 and the scan spatial resolution was 6 mm. The surface was scanned twice by the ToF camera. Then 100 – 450 cm^3 of sediment was manually extracted from the mound. The volume of the extracted sediment was measured by a measuring cup. After extraction, the surface was again scanned twice by the camera. The experiment was repeated 45 times with varying amounts of extracted sediment. The scans were transformed to point clouds in VoxelViewer-0.9.10, and the point clouds were corrected according to Eq. (2) and (3). The *z*-coordinates of the two point clouds before and two point clouds after the extraction were averaged. The point clouds were then transformed into DSMs, and the differences between the time steps were calculated. A scan was taken of a smooth surface, and the standard deviation of its *z*-coordinates was calculated and saved as a threshold value. Solely, the differences between the DSMs below this threshold (0.2 cm) were considered in the calculation of the detected sediment extraction. The detected extracted sediment volume was then calculated for each experiment as follows:

$$Vol_{detected} = \sum_{p}^{1}\left(DSM_{before} - DSM_{after}\right) * res^2 \quad , \qquad (4)$$

In Eq. (4), $Vol_{detected}$ is the volume of the extracted sediment as detected by the camera (cm^3), p is the number of pixels, DSM_{before} (cm) is the DSM calculated from the scan taken before the extraction, DSM_{after} (cm) is the DSM calculated from the scan taken after the extraction, res (cm) is the resolution of the scan, which was 0.6 cm. To evaluate the camera's accuracy, the measured volume of the extracted sediment was compared to the volume detected by the camera. The camera's accuracy was estimated between the detected volume and measured volume as follows:

$$MAE = \sum_{1}^{n} \frac{(Vol_{detected} - Vol_{measured})}{area} \quad . \qquad (5)$$

In Eq. (5), MAE (cm^3/cm^2) is the mean absolute error, n is the number of scans, $Vol_{measured}$ (cm^3) is the volume of the extracted sediment measured by the measuring cup, and the area is the total surface area monitored by the camera (cm^2).

3.4 Installation of the cameras in the field

We installed 8 custom-tailored ToF-based cameras on 4 hillslopes in two climate zones in areas including visible signs of bioturbation activity (burrows) and areas without visible signs of bioturbation (Fig. 2). The cameras were installed in LC on the north-facing upper hillslope (LC-NU), north-facing lower hillslope (LC-NL), south-facing upper hillslope (LC-SU) and the south-facing lower hillslope (LC-SL); in PdA on the north-facing upper hillslope (PdA-NU), north-facing lower hillslope (PdA-NL), south-facing upper hillslope (PdA-SU) and south-facing lower hillslope (PdA-SL). The custom-tailored cameras were installed during a field campaign in March 2019, the monitoring took place for seven months, and the data were collected in October 2019. The

https://doi.org/10.5194/esurf-2021-104
Preprint. Discussion started: 11 January 2022
© Author(s) 2022. CC BY 4.0 License.

construction consisted of a 3D ToF-based sensor from Texas Instruments (Li, 2014), a RasperryPi single board computer (SBC), a timer, a 12 V 12 Ah battery and three 20 W solar panels for unattended operation (Fig. 1). Solar panels were located at the camera pole and were recharging the battery via a charge controller. The camera was located approximately one meter above the surface, facing the surface with a tilt angle of 10 degrees. The timer was set to close the electric circuit 4 times a day: at 1 a.m., 5 a.m., 8 a.m. and 10 p.m. At these times, the camera and the computer were turned on for 15 minutes. The camera turned on and took five scans delayed one second from each other and sent them to the SBC. Each camera had its own WiFi (Wireless Fidelity) and the data could be read from the SBC via Secure Shell (SSH).

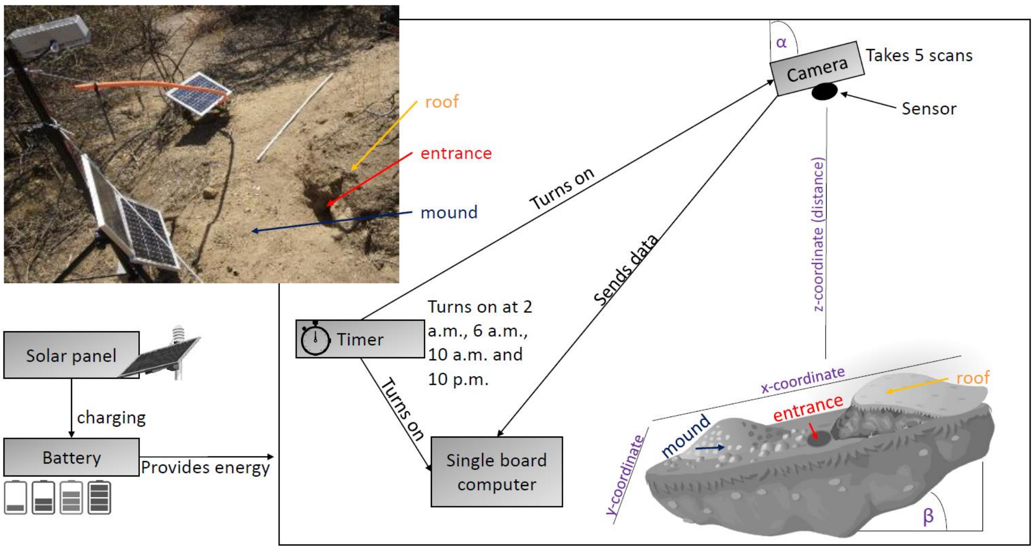

Figure 2. Scheme and photo example of a Time-of-Flight-based camera installation in the field. The photo example is from upper north-facing hillslope in La Campana. Black boxes describe single installation parts. Purple descriptions are the variables needed for the correction of the scans. Roof, entrance and mound describe areas affected by the burrowing animal. The *x*-, *y*- and *z*-coordinates are 3D coordinates identifying the position of each point in space, where the *x*-coordinate is the length, *y*-coordinate is the width and the *z*-coordinate is the distance between the camera sensor and the surface. α is the inclination of the camera, and β is the surface inclination.

3.5 Delineation of the Area Affected and Non-Affected by Burrowing Animals in the Camera's Field of View

The surface area scanned by the cameras was divided by a delineation scheme into areas affected (A) and not (directly) affected (N) by burrowing animals. The affected areas included three sub-areas: (i) mound (M), (ii) entrance (E) and (iii) burrow roof (R). "Mound" describes the sediment excavated by the animal while digging the burrow. "Entrance" describes the entry to the animal burrow up to the depth possible to obtain via the camera. "Burrow roof" describes the part of the sediment above and uphill the burrow entrance (Bancroft et al., 2004). During the burrow's creation, sediment was not only excavated but also pushed aside and uphill the entrance, which created the burrow's roof. We assume that this elevated microtopographical feature then

https://doi.org/10.5194/esurf-2021-104
Preprint. Discussion started: 11 January 2022
© Author(s) 2022. CC BY 4.0 License.

Earth Surface Dynamics Discussions
Open Access
EGU

forms an obstacle for sediment transported from uphill, which leads to its accumulation in this area. The remaining surface within the camera's FOV was classified as not affected (N) by the burrowing animal during the creation of its burrow.

For the delineation, we used the DSM calculated from the point cloud, and a slope layer calculated from the DSM (Horn, 1981). Entrance was assigned to an area determined by a search algorithm starting at the lowest point of the DSM (pixel with the highest *z*-coordinate value). We increased the circular buffer around the starting point by one pixel until the average depth of the new buffer points was not higher than the height of the camera above the surface, or until the slope of at least 50% of the new buffer points was not 0. Then, we masked all pixels within the buffer with a depth lower than the average depth of the points within the buffer, which had a slope that was 0. The remaining pixels belonged to the entrance area. Then, the surface scan was divided into an uphill and downhill part with regards to the entrance position. Both the uphill and the downhill parts were subdivided into 16 squares.

To delineate the mound in the downhill part, we first identified the highest points (pixel with the lowest *z*-coordinate value) within all 16 squares. We then calculated the distance of these maxima to the entrance, and the pixel located nearest to the entrance was identified as the highest point of the mound (i.e., seed point). Consecutively, we increased the circular buffer around the seed point by one pixel until the average depth of the new buffer points was not lower than the height of the camera above the surface, or until the slope of at least 50% of the new buffer points was not 0. Then, we masked all pixels within the buffer with a depth higher than the average depth of the points within the buffer, which had a slope that was 0. The remaining pixels were classified as mound area. To delineate burrow roof, we used the same approach as for the delineation of mound and applied it on the uphill part of the surface scan. All pixels that were not classified during the entire delineation process were treated as areas not affected by animals. The position and the boundaries of entrance, mound and burrow roof were validated visually (Fig. 3 and A1).

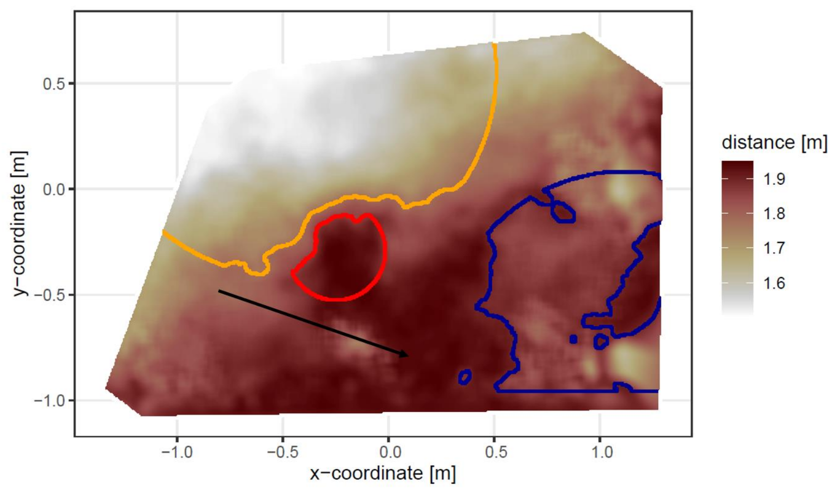

Figure 3. Corrected digital surface model of the camera on the upper north-facing hillslope in La Campana with delineated areas. The point of origin of the coordinate system is at the camera nadir. Distance refers to the distance between surface and camera. The red line delineates the burrow entrance, blue the mound and

orange the burrow roof. The area which was outside of any delineated area was classified as not affected by animal burrowing activity. The arrow indicates a downhill direction of the hillslope.

3.6 Calculation of daily sediment mass balance budget

The volume of the redistributed sediment was calculated daily and was then cumulated from the first day of monitoring. For the calculation of the daily sediment redistribution, the change in the surface level detected by the camera was calculated first. For each day, the scans from the day before and after the respective day were averaged and subtracted. As described in Section 2.2., all values with a difference below and above the threshold value of 0.2 cm were set to 0. The redistributed sediment volume was then calculated from the surface change for each pixel as follows:

$$Vol_{redistributed} = (S_b - S_a) * res^2 \quad . \qquad (6)$$

In Eq. (6), $Vol_{redistributed}$ (cm^3 $pixel^{-1}$) is the volume of the calculated redistributed sediment, S_b (cm) the scan before, S_a (cm) the scan after the rainfall event and *res* is the spatial resolution (cm). Using the daily volume of the redistributed sediment per pixel, we calculated the daily mass balance budget by summing the volume of sediment eroding or accumulating within each delineated area.

3.7 Calculation of animal-caused and rainfall-caused sediment redistribution

The animal-caused sediment redistribution occurred when the animal actively reworked sediment within its burrow. Under the assumption that the burrows are actively used by the animals, we defined four cases when the sediment was redistributed due to the burrowing activity. For this, we pairwise compared the DSMs of each scan with the scan saved before. The four cases were: (i) as the animal excavates sediment from the entrance, the depth of the entrance must increase in the second scan; (ii) as the excavated sediment accumulates on the mound, the height of the mound must increase in the second scan; (iii) as the burrowing might lead to an expansion or a collapse of the burrow roof, an increase or decrease of the burrow roof must occur between the scans; (iv) as the animal only digs within his burrow, no changes must occur between the two scans within the area not affected by the animal. The animal-caused redistribution was then calculated for these days as the volume of sediment redistributed within mound and burrow roof. The entrance was ignored in the calculation. As the sediment excavated from the entrance accumulated on the mound and the sediment accumulated within entrance collapsed from the burrow roof, by including the entrance in the calculation, these sediment volumes would be counted twice.

The rainfall-caused sediment redistribution was calculated as follows: From the data from the climate stations (Übernickel et al., 2021a), we calculated the daily precipitation in mm. The sediment redistribution recorded immediately and within five scans before and after a rainfall event is defined to be the result of the rainfall event. The five-scan buffer is necessary as the climate stations are located up to a 15 km distance from the cameras (Fig. 1). We calculated the rainfall-caused sediment redistribution within (i) areas affected by the burrowing animal (i.e., entrance, mound and burrow roof) and (ii) within areas not affected by the burrowing animal. To estimate the sediment volume which accumulated within the entrance, we also calculated the volume of redistributed sediment solely (iii) within the mound and burrow roof. From this volume, we subtracted the volume redistributed within all affected areas. We did not directly calculate the accumulation rate within the entrance as the cameras did not provide data on the complete underground burrow structure.

3.8 Hillslope-wide upscaling of redistributed sediment

https://doi.org/10.5194/esurf-2021-104
Preprint. Discussion started: 11 January 2022
© Author(s) 2022. CC BY 4.0 License.

Hillslope-wide upscaling of the results generated in this study was performed by utilising a previous estimation of vertebrate burrow density (Grigusova et al., 2021). In this study, the density of burrows created by vertebrate burrowing animals, which we interpreted as vertebrate burrow density (number of burrows per 100 m^2), was measured in situ within eighty 100 m^2 plots and then upscaled to the same hillslopes on which the cameras were located by applying machine-learning methods, using the UAV-data as predictors. Hence, the modelled burrows in the previous study were in fact areas affected by burrowing animals in this study.

From the camera data, we calculated the average cumulative volume of redistributed sediment after a period of one year within affected ($Vol_{affected}$ ($cm^3\ cm^{-2}\ year^{-1}$)) and non-affected ($Vol_{not\ affected}$ ($cm^3\ cm^{-2}\ year^{-1}$)) areas and the average sediment volume redistributed (excavated) by the animal (Vol_{exc} ($cm^3\ cm^{-2}\ year^{-1}$)), separately for each site. Additionally, we estimated the volume of sediment that was additionally redistributed during rainfall events due to the presence of the burrow (Vol_{add} ($cm^3\ cm^{-2}\ year^{-1}$)). Vol_{add} was calculated as the difference in the redistributed sediment volume between affected and non-affected areas according to Eq. (7).

$$Vol_{add} = \frac{(M_{affected} - M_{unaffected})}{7} * 12 \quad , \tag{7}$$

We then upscaled the $Vol_{affected}$ ($cm^3\ cm^{-2}\ year^{-1}$), Vol_{exc} ($cm^3\ cm^{-2}\ year^{-1}$)) and Vol_{add} ($cm^3\ cm^{-2}\ year^{-1}$)) to the hillslope using the same approach: First, we calculated the average volume of the redistributed sediment per burrow ($Vol_{per\ burrow}$ [$cm^3\ burrow^{-1}\ year^{-1}$]):

$$Vol_{per\ burrow} = \frac{(Area_{burrow} * Vol)}{7} * 12 \tag{8}$$

In Eq. (8), $Area_{burrow}$ (cm^2) is the average size of the burrows that are monitored by the cameras; Vol is $Vol_{affected}$ ($cm^3\ cm^{-2}\ year^{-1}$), Vol_{exc} ($cm^3\ cm^{-2}\ year^{-1}$) or Vol_{add} ($cm^3\ cm^{-2}\ year^{-1}$). Using the hillslope-wide predicted vertebrate burrow densities ($Dens_{burrow}$ (number of burrows 100 m^{-2})) from Grigusova et al. 2021, we estimated the volume of redistributed sediment for each pixel of the raster layers ($Vol_{per\ pixel}$ ($cm^3\ m^{-2}\ year^{-1}$)) according to Eq. (9):

$$Vol_{per\ pixel} = \frac{Vol_{per\ burrow} * Dens_{burrow}}{7} * 12 \tag{9}$$

The average hillslope-wide volume of redistributed sediment ($Vol_{hillslope\text{-}wide}$ ($m^3\ ha^{-1}\ year^{-1}$)) was then estimated as follows:

$$Vol_{hillslope-wide} = \frac{\sum_1^m Vol_{per\ pixel}}{7} * 12 * 0.001 \quad , \tag{10}$$

In Eq (10), m is the number of pixels.

4. Results

4.1 Camera accuracy

The accuracy between the measured extracted sediment volume and sediment volume calculated from the camera scans was very high (MAE = 0.023 $cm^3\ cm^{-2}$, R^2 = 0.77, Fig. 4). The accuracy between the calculated and measured extracted sediment was higher when the two scans taken before as well as after the extraction of the sediment were averaged and the sediment volume was estimated using these averaged scans. When calculating the redistributed sediment from solely one scan before and after extraction, the accuracy slightly decreased (MAE = 0.081 $cm^3\ cm^{-2}$, R^2 = 0.64). The cameras tended to overestimate the volume of redistributed sediment.

https://doi.org/10.5194/esurf-2021-104
Preprint. Discussion started: 11 January 2022
© Author(s) 2022. CC BY 4.0 License.

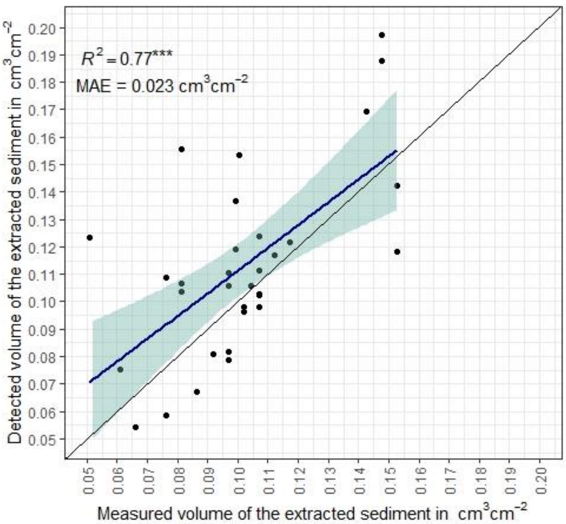

Figure 4. Estimation of Time-of-Flight camera accuracy based on averaging two surface scans before and after the sediment extraction under controlled conditions. The *x*-axis shows the exact sediment volume measured with a cup. The *y*-axis represents the volume of the sediment calculated from the camera scans (according to Equation (4)). The blue line is the linear regression calculated from the measured and detected volume. The green shadow shows the confidence interval of 95% for the linear regression slope. ***$p \leq 0.001$. MAE is the mean absolute error, and R^2 the coefficient of determination.

4.2 Data quantity and quality

Six out of eight custom-tailored cameras collected data over the seven-month period (Table A2). One camera collected data for a period of three months and one camera stopped working a few days after installation. The quantity of usable point clouds taken at 1 a.m., 5 a.m. and 10 p.m. was higher than of point clouds taken at 8 a.m. Approximately 20% of points was removed from the point clouds before final analysis due to the high scattering at the point cloud corners. After data filtering (see Section 3.2.), 1326 scans were usable and for 86% of the days, at least one usable scan was available. The usable scans were distributed continuously within the monitoring period.

In LC, the areas affected by the burrowing animal always consisted of an entrance, mound and burrow roof. In PdA, there was no burrow roof on the upper hillslopes. Burrows without a burrow roof were located on shallower parts of the hillslopes (up to an inclination of 5°), and the angle of the burrow entrance to the ground was ~90°. Burrows with a burrow roof were located on steeper parts of the hillslopes (with an inclination above 5°), and the angle of the burrow entrance to the ground was ~45°.

4.3 Mass balance of redistributed sediment

The cameras detected (i) sediment redistribution directly following rainfall events and (ii) due to the burrowing activity in times without rainfall (Fig. 5 and 6). In all cases, areas affected by burrowing activity (entrance, burrow roof and mound) exhibited higher sediment redistribution rates than areas not affected by burrowing. In addition, the volume of redistributed sediment by animal activity was higher after a rainfall event

https://doi.org/10.5194/esurf-2021-104
Preprint. Discussion started: 11 January 2022
© Author(s) 2022. CC BY 4.0 License.

occurred. After rainfall events, sediment eroded especially at the boundaries of the burrow roof and mound. Sediment eroded from the burrow roof accumulated within the burrow entrance or was redistributed to the mound (Fig. 7). We can also identify detected sediment accumulation on the upper parts of the burrow roof. After the burrowing activity, sediment was excavated from the entrance and cameras detected accumulation on the mound and within the burrow roof. The sediment accumulation and erosion within the area not affected by the animal was evenly distributed around the burrow (Fig. 7).

In the following, the dynamics are exemplarily explained for four cameras. Animal burrowing activity was detected seven times by the camera LC NU (Fig. 5a, A2a and A3a) during the monitoring period, by an increase in sediment volume in the area delineated as mound. Simultaneously, the burrow entrance showed signs of modification and sediment accumulation, but these changes were less clear. Overall, the volume of the excavated soil varied. From April until June, up to 0.5 cm^3 cm^{-2} of sediment was excavated by the animal and accumulated on the mound. From June until September, animal burrowing activity was detected at four time slots (5 June 2019, 9 June 2019, 1 July 2019 and 18 August 2019) and sediment volume of up to 2 cm^3 cm^{-2} accumulated each time on the mound, burrow roof and within the entrance. During the rainfall events of up to 20 mm day^{-1} on 16 June 2019, 27 mm day^{-1} on 29 June 2019 and 7 mm day^{-1} on 13 July 2019, sediment volume of up to 4 cm^3 cm^{-2} eroded, especially from the burrow roof and the mound while a sediment volume of up to 1 cm^3 cm^{-2} accumulated within the entrance during each rainfall event.

Camera LC-SL (Fig. 5b and A3b) showed burrowing activities eight times and sediment volumes of up to 3 cm^3 cm^{-2} accumulated within the entrance and burrow roof. The camera detected sediment erosion of up to 2 cm^3 cm^{-2} after a rainfall event of 27 mm day^{-1} on 27 July 2019. On the south-upper hillslope, the camera detected animal burrowing activity six times, with a sediment accumulation of up to 3 cm^3 cm^{-2} (Fig. A2 and A3).

In contrast, camera PdA-NU pointed to animal burrowing activity up to 15 times where up to 1 cm^3 cm^{-2} of sediment volume was redistributed from the entrance to the mound (Fig. 6a, A2e and A3e). At the end of June on 27 June 2019, a rainfall event of 1.5 mm day^{-1} occurred and up to 2 cm^3 cm^{-2} of sediment eroded from the burrow roof and accumulated within the burrow entrance. We observed increased sediment redistribution by the animal after the rainfall events.

Camera PdA-SL evenly revealed animal burrowing activity up to 15 times (Fig. 6b, A2f and A3f). The burrowing had a strong effect on the sediment redistribution. The rainfall event of 1.5 mm day^{-1} on 27 June 2019 did not cause any detectable surface change.

https://doi.org/10.5194/esurf-2021-104
Preprint. Discussion started: 11 January 2022
© Author(s) 2022. CC BY 4.0 License.

Earth Surface Dynamics
Discussions
Open Access
EGU

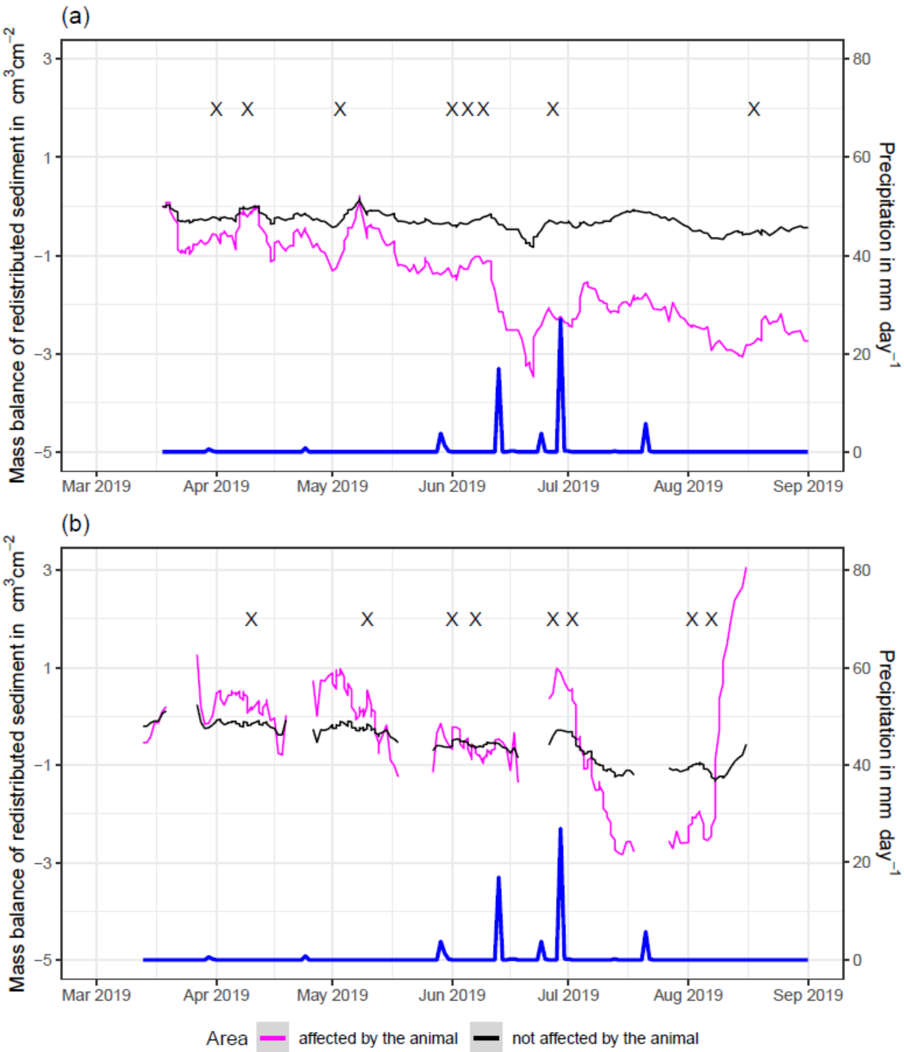

Figure 5. Examples of mass balance of redistributed sediment in mediterranean La Campana for areas affected and not affected by burrowing animals: (**a**) The record of the camera on the upper north-facing hillslope showed that larger rainfall events cause a negative sediment balance (sediment loss), followed by a phase of positive sediment mass balance after approximately 3 days due to the fact of sediment excavation; (**b**) The record of the camera on the lower south-facing hillslope showed a similar pattern to the camera on the upper north-facing hillslope, but the phase of positive mass balance was delayed in comparison. The blue line is the daily precipitation in mm day^{-1}, and "X" marks the days at which animal burrowing activity was detected. Mass balances for all cameras are displayed in Fig. A2 and A3.

https://doi.org/10.5194/esurf-2021-104
Preprint. Discussion started: 11 January 2022
© Author(s) 2022. CC BY 4.0 License.

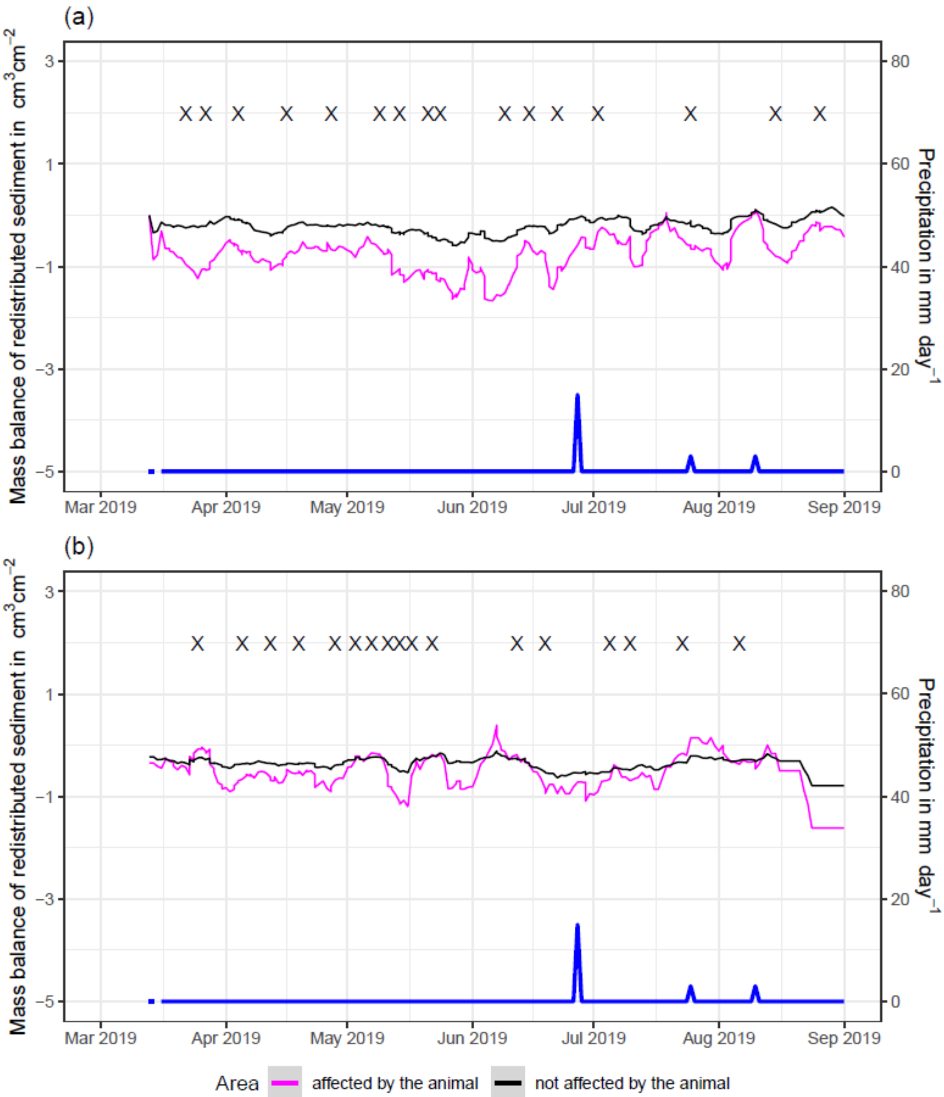

Figure 6. Examples of mass balance of redistributed sediment in the arid Pan de Azúcar for areas affected and not affected by burrowing animals: (**a**) The record of the camera on the upper north-facing hillslope showed that animal sediment excavation had a larger impact on the mass balance than rainfall events; (**b**) The record of the camera on the lower south-facing hillslope showed a similar pattern to the camera on the upper north-facing hillslope. The blue line is the daily precipitation in mm day^{-1}, and "X" marks the days at which animal burrowing activity was detected. Mass balances for all cameras are displayed in Fig. A2 and A3.

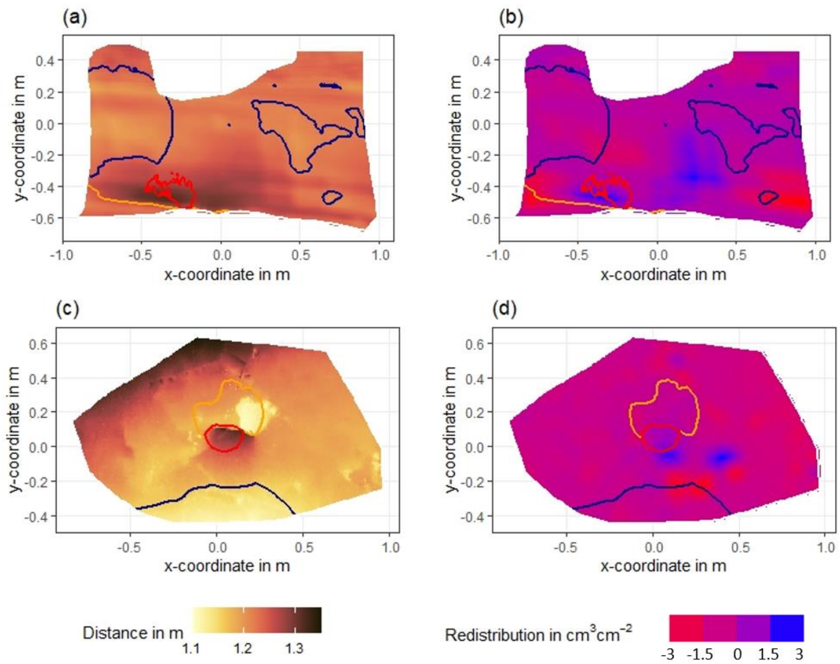

Figure 7. Examples of surface scans showing the digital surface model (DSM) before a rainfall event (**a**, **c**) at two camera locations in La Campana, and the calculated volume of redistributed sediment (**b**, **d**) after the rainfall event: (**a**) DSM of a scan from the camera on the upper north-facing hillslope in La Campana; (**b**) Detected sediment redistribution ($cm^3\ cm^{-2}$) on the upper north-facing hillslope in La Campana after a rainfall event of 17.2 mm day^{-1}; (**c**) DSM of a scan from the camera on the upper south-facing hillslope in La Campana; (**d**) Detected sediment redistribution ($cm^3\ cm^{-2}$) on the upper south-facing hillslope after a rainfall event of 17.2 mm day^{-1}. Red is the outline of the burrow entrance. Green is the outline of mound. Orange is the outline of the burrow roof. The area which is not outlined is the area not directly affected by animal burrowing activity. Redistribution is the volume of the redistributed sediment, either accumulated (positive value) or eroded (negative value) per $cm^3\ cm^{-2}$. After the rainfall events, sediment mostly accumulated within the burrow entrance or near mounds and eroded from burrow roofs and mounds.

4.4 Cumulative volume of redistributed sediment

The analysis of cumulative volume of the redistributed sediment caused by burrowing animal activity and rainfall over the monitored period of seven months for all eight cameras showed a heterogeneous pattern (Fig. 8 and A4, Tables A3 and A4).

In LC, the cumulative volume of the sediment excavated by the animal within the burrow roof and mound increased continuously (Fig. 8). Especially between the rainfall events from June until August, a cumulative volume of on average 6.5 $cm^3\ cm^{-2}$ was excavated by the animal. We calculated that, on average, 8.53 $cm^3\ cm^{-2}$ cumulatively eroded from the burrow roof and mound; while 2.44 $cm^3\ cm^{-2}$ sediment volume accumulated within the entrance (Fig. 8). These results indicate that 28% of sediment eroding from the burrow roof accumulated within the entrance, while over 62% of sediment eroded downhill. Averaged over all camera

https://doi.org/10.5194/esurf-2021-104
Preprint. Discussion started: 11 January 2022
© Author(s) 2022. CC BY 4.0 License.

Earth Surface Dynamics
Discussions
Open Access
EGU

scans, 338% more sediment was redistributed by rain within the affected area compared to the non-affected area (Fig. 9).

In PdA, cameras continuously detected animal burrowing activity and excavation of the sediment (Fig. A4). The volume of the detected excavated sediment increased steadily within all cameras. The cumulative sediment accumulation surpasses the sediment eroded due to the rainfall. The volume of the sediment eroded within the affected areas was 40% higher than within the non-affected areas (Fig. 9). The results show that approximately 50% of the eroded sediment accumulated within the entrance.

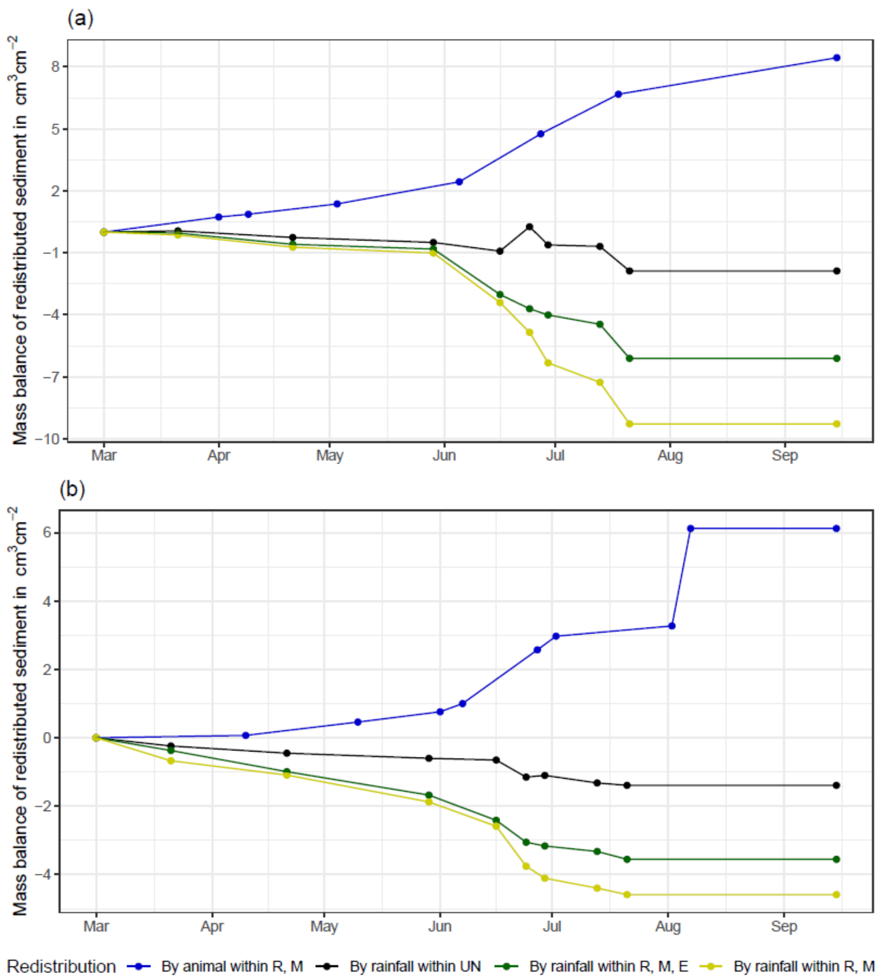

Figure 8. Examples of the cumulative volume of redistributed sediment within affected and non-affected areas caused by animal burrowing activity or rainfall in mediterranean La Campana: (**a**) Upper north-facing hillslope; (**b**) Lower south-facing hillslope. Positive values indicate sediment accumulation. Negative values indicate sediment erosion. E is the burrow entrance; M is the mound; R is burrow roof; UN is the area not directly affected by the animal burrowing activity. Cumulative volumes for all cameras are in Fig. A4.

https://doi.org/10.5194/esurf-2021-104
Preprint. Discussion started: 11 January 2022
© Author(s) 2022. CC BY 4.0 License.

Earth Surface Dynamics
Discussions
Open Access
EGU

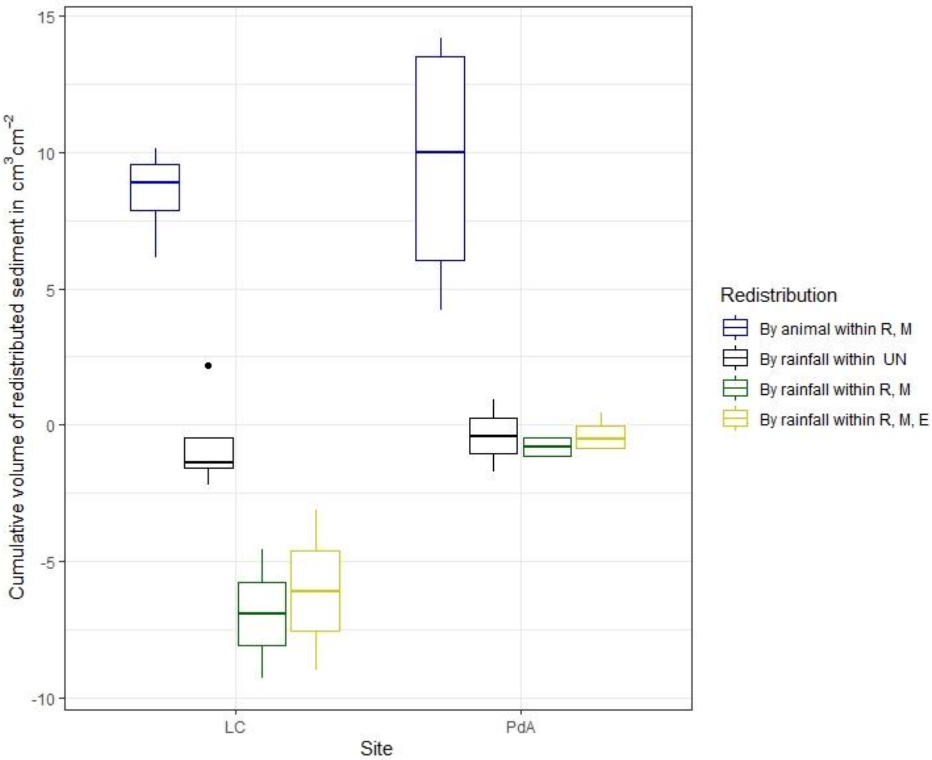

Figure 9. Cumulative volume of the redistributed sediment for all cameras. Positive values indicate sediment accumulation. Negative values indicate sediment erosion. Whiskers indicate the median of sediment redistribution. E is the burrow entrance; M the mound; R is the burrow roof; UN is area not affected by the animal burrowing activity; LC stands for National Park La Campana in the mediterranean climate zone; PdA stands for National Park PdA in the arid climate zone.

4.5 Hillslope wide excavation and redistribution

Grigusova et al. (2021) showed that the density of vertebrate burrows was between 6 and 12 per 100 m^2 in LC and between 0 and12 per 100 m^{-2} in Pan de Azúcar. The volume of the sediment excavated by the animal and redistributed during rainfall events varied between sites and across the hillslopes (Fig. 10, A5 and A6; Tables A3 and A4).

The volume of the sediment excavated by the animal per burrow was lower in LC (1226.61 cm^3 burrow^{-1} year^{-1}) than in PdA (1498.66 cm^3 burrow^{-1} year^{-1}) (Fig. 9, Table 1). However, on the hillslope scale, a higher total area-wide volume of excavations was calculated for LC compared to PdA (0.67 m^3 ha^{-1} year^{-1} vs. 0.18 m^3 ha^{-1} year^{-1}), due to the higher burrow density in LC.

The volume of the sediment redistributed within the area affected by burrowing activity during rainfall events on the hillslope scale was higher in LC (–0.48 m^3 ha^{-1} year^{-1}) than in PdA (–0.05 m^3 ha^{-1} year^{-1}) (Table 1). The volume additionally redistributed sediment due to the presence of the burrows was well higher in LC than in PdA (Fig. 10, A5 and A6).

The hillslope-wide redistribution rates increased with burrow density, which, as stated in Grigusova et al. (2021), largely depends on vegetation distribution and topography. In LC, more sediment was excavated in

© Author(s) 2022. CC BY 4.0 License.

parts of the hillslope with a vegetation cover of over 50% m^{-2} (~0.60 $m^3\,ha^{-1}\,year^{-1}$) than in non-vegetated parts of the hillslope (~0.2 $m^3\,ha^{-1}\,year^{-1}$). However, dense vegetation covers over 80% m^{-2} reduced volume of redistributed sediment due to the animals' burrowing activity (Fig. A5, A7c and A7d). More sediment was redistributed in the middle and upper parts of the hillslope (Fig. A5, A7a and A7b). In PdA, the volume of sediment redistributed by the burrowing animals increased with vegetation cover and elevation (Fig. A6 and A8).

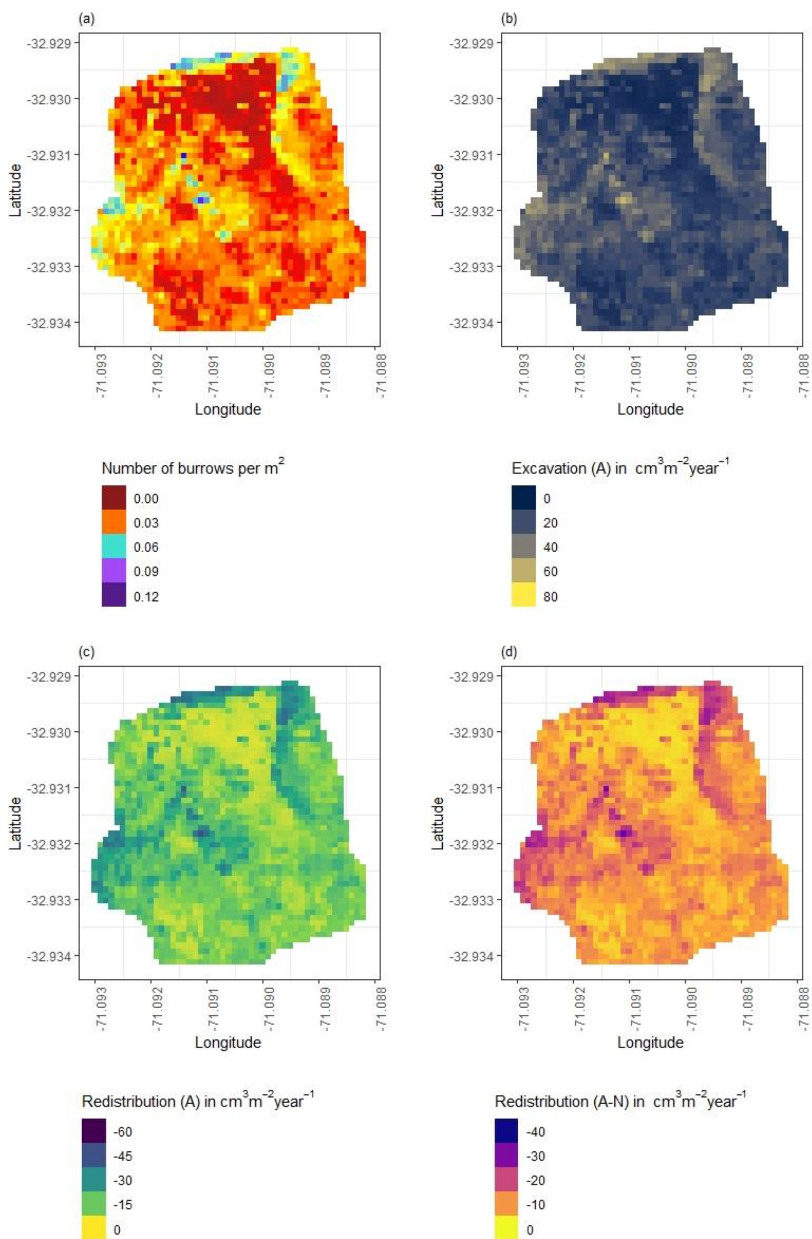

https://doi.org/10.5194/esurf-2021-104
Preprint. Discussion started: 11 January 2022
© Author(s) 2022. CC BY 4.0 License.

Figure 10. Example of the hillslope-wide volume of redistributed sediment for a time period of one year on the south-facing hillslope in La Campana: (a) Density of burrows as estimated by Grigusova et al. (2021); (b) Volume of the sediment excavated by the animals; (c) Volume of the sediment redistributed during rainfall events within affected areas; (d) Volume of additionally redistributed sediment during rainfall events due to the presence of the burrows. The values were calculated per burrow as stated in Section 3.7. by subtracting the sediment volume redistributed within animal-affected areas from the sediment volume redistributed within non-affected area and then upscaled. The letters in brackets indicate if the upscaling was conducted using data from affected or non-affected areas by burrowing animals. “A” stands for affected area. By “A-N”, the redistribution calculated from non-affected areas was subtracted from the redistribution calculated within affected areas to obtain the additional volume of redistributed sediment due to the burrows’ presence.

Table 1. Summary of the volume of redistributed sediment according to site, area, and disturbance type. Vol_{exc} describes the volume of the sediment excavated by the animals. $Vol_{affected}$ describes the volume of the sediment redistributed during rainfall events within affected areas. Vol_{add} describes the volume of additionally redistributed sediment during rainfall events due to the presence of the burrows. The values were calculated per burrow, as stated in Section 3.7., by subtracting the sediment volume redistributed within animal-affected areas from the sediment volume redistributed within non-affected areas and then upscaled.

Variable		**Volume of redistributed sediment**	
Disturbance	Area	LC	Pan de Azúcar
Vol_{exc}	Affected area	14.62 cm^3 cm^{-2} $year^{-1}$	16.41 cm^3 cm^{-2} $year^{-1}$
	Per burrow	1226.61 cm^3 $burrow^{-1}$ $year^{-1}$	1498.66 cm^3 $burrow^{-1}$ $year^{-1}$
	Hillslope-wide	0.67 m^3 ha^{-1} $year^{-1}$	0.18 m^3 ha^{-1} $year^{-1}$
$Vol_{affected}$	Affected area	–10.44 cm^3 cm^{-2} $year^{-1}$	–1.41 cm^3 cm^{-2} $year^{-1}$
	Per burrow	–876.38 cm^3 $burrow^{-1}$ $year^{-1}$	–126.36 cm^3 $burrow^{-1}$ $year^{-1}$
	Hillslope-wide	–0.48 m^3 ha^{-1} $year^{-1}$	–0.05 m^3 ha^{-1} $year^{-1}$
Vol_{add}	Affected area	–7.37 cm^3 cm^{-2} $year^{-1}$	–1.18 cm^3 cm^{-2} $year^{-1}$
	Per burrow	–619.2 cm^3 $burrow^{-1}$ $year^{-1}$	–48.36 cm^3 $burrow^{-1}$ $year^{-1}$
	Hillslope-wide	-0.34 m^3 ha^{-1} $year^{-1}$	-0.02 m^3 ha^{-1} $year^{-1}$

5. Discussion

Our results showed that the new ToF device is a suitable tool for high-resolution, autonomous monitoring of surface changes, applicable also in remote areas. The ability of a continuous observation of sediment redistribution over a longer time during our study provided new insights into the importance of burrowing animals for sediment redistribution. Our research reveals that the presence of vertebrate burrows increases hillslope sediment redistribution rates much more than previously assumed (up to 208%). We showed that the quantity of animal-related sediment redistribution, however, varied on rainfall occurrence, with an increase in sediment redistribution between 40% in the arid research area and 338% percent in the mediterranean research area.

5.1 Suitability of the ToF method for surface monitoring

https://doi.org/10.5194/esurf-2021-104
Preprint. Discussion started: 11 January 2022
© Author(s) 2022. CC BY 4.0 License.

Earth Surface Dynamics Discussions

The here proposed monitoring technique enables an automatic monitoring of surface changes on a microtopographic scale, and its measurement continuity allows for the analysis of ongoing biogeomorphological processes in high temporal resolution.

Our ToF device stands in contrast to earlier studies that used laser scanning technology to monitor microtopographic changes, with regard to the costs, measurement frequency and sampling autonomity (Table A5).

Previous authors mainly applied expensive laser scanning for the estimation of sediment redistribution, and the research sites had to be personally revisited for each of the measurements (Nasermoaddeli and Pasche, 2008; Eltner et al., 2016b; Eltner et al., 2016a; Hänsel et al., 2016). In contrast to other laser scanning methods (Table A5), our approach is instrumentally much more cost-effective and, thus, easier to apply and more available also for smaller case studies with multiple objects to be observed at the same time. The cost for the laser scanners and needed equipment used in previous studies varied between USD 4500 and up to USD 240,000 (Nasermoaddeli and Pasche, 2008; Morris et al., 2011) (Table A5). In comparison, the cost of our ToF system comprises only USD 900, which is a 5–240 times lower price.

In terms of data quality, our ToF device is more precise or comparable to those employed in other studies. The accuracy of the camera (R^2 = 0.77) was in the range of previous studies (R^2 = 0.26–0.83 (Eitel et al., 2011), Table A5). The horizontal point spacing of our cameras was 0.32 cm, and the maximum number of points per cm^2 was 8.5. These values are similar to previous studies in which the used devices had a horizontal point spacing in the range of 0.25–0.57 cm (Kaiser et al., 2014; Nasermoaddeli and Pasche, 2008)) (Table A5), and the maximum number of points per cm^2 in a range of 1 point–25 points cm^{-2} (Eitel et al., 2011; Longoni et al., 2016) (Table A5).

Our cameras tended to slightly overestimate or underestimate the volume of redistributed sediment. This error occurs when the pulse reflects from several vertical objects such as walls or, in our case, branches or stones and then enters the camera sensor. This phenomenon was also observed in previous studies applying laser scanners and is inevitable if the goal is to study surface changes under natural field conditions (Kukko and Hyyppä, 2009; Ashcroft et al., 2014). During operation of the cameras, we learnt that our newly developed instruments are particularly capable of delivering usable scans at night. This is likely due to the strong scattered sunlight reaching the camera sensor during the day, blurring the data (Li, 2014). Thus, we recommend focusing on nocturnal operation to prevent light contamination from the surroundings.

We could thus prove that the ToF cameras are a suitable and cost-effective method for a continuous monitoring of sediment redistribution at a microtopographic scale without the need of expensive laser scanning campaigns.

5.2. Sediment Redistribution

Our research reveals that the presence of vertebrate burrows generally increases hillslope sediment redistribution. We show, however, that the ratio between the sediment redistribution caused by rainfall in the areas affected and not affected by burrowing animals varies between the climate zones. The sediment redistribution in the affected areas was 40% higher in the arid research site, and in the mediterranean research site, it was 338% higher when compared to the areas not affected by burrowing animals (Fig. 9, Tables A3 and A4).

By monitoring microtopographical changes in a high spatio-temporal resolution, we found that the occurrence of larger rainfall events played a two-fold, accelerating role in influencing sediment redistribution

https://doi.org/10.5194/esurf-2021-104
Preprint. Discussion started: 11 January 2022
© Author(s) 2022. CC BY 4.0 License.

(Fig. A3 and A4). Firstly, rainfall-runoff eroded burrow material causing increased sediment loss. Ultimately, after the rainfall, the cameras detected animal burrowing activity. The rainfall triggered the burrowing activity which was likely related to a lower burrowing resistance of the soil due to the increased soil moisture (Rutin, 1996; Romañach et al., 2005; Herbst and Bennett, 2006). This double feedback led to frequently occurring but small redistribution rates. However, cumulatively, this mechanism increased downhill sediment fluxes. Previous studies most likely missed this low magnitude but frequent surface processes and, thus, did not estimate the full volume of redistributed sediment due to the fact of their sporadically taken measurements. To quantify all occurred sediment redistribution processes, a continuous frequent surface monitoring, like the here presented, is needed.

In contrast to our result, the maximum increase in the sediment volume redistributed during rainfall events measured in the areas affected by burrowing animals when compared to not affected areas was 208% ((Imeson and Kwaad, 1976) Table A6). Our results, however, indicate an increase of up to 338% (Table 9). This means, that the contribution of animals' (vertebrates') burrowing activity in the mediterranean climate appear larger than previously observed by using field methods such as erosion pins or splash traps (–3 – 208%, (Imeson and Kwaad, 1976; Hazelhoff et al., 1981; Black and Montgomery, 1991) , Table A6). In contrast, in arid PdA, our study found a much smaller increase (40%, Fig. 9) in the sediment volume redistributed during rainfall events measured in the areas affected by burrowing animals when compared to not affected areas. This is lower than previously estimated (125%, (Black and Montgomery, 1991), Table A6). However, solely one rainfall event above 0.2 mm day^{-1} occurred during our monitoring period. Hence, we conclude that the contribution of burrowing activity of animals to hillslope sediment transport is much larger in areas with frequent rainfall events than previously thought, while it has been realistically estimated by previous studies for areas with rare rainfall events (Table A6).

Overall, our study revealed a strong impact of animal excavation processes on sediment redistribution in the mediterranean climate zone (0.67 m^3 ha^{-1} year^{-1}), which were more in a range of excavated volume observed in previous studies by bears and porcupines (0.49 m^3 ha^{-1} year^{-1}, (Hall et al., 1999), Table A8) than rodents (0.02 m^3 ha^{-1} year^{-1}, (Hall et al., 1999)). The estimated sediment excavation in the arid climate zone (0.18 m^3 ha^{-1} year^{-1}, Fig. A4, Table A8) was in the order of magnitude of previous studies (0.05–0.2 m^3 ha^{-1} year^{-1}, (Black and Montgomery, 1991; Yoo et al., 2005), Table A8). Our results thus suggest that animal burrowing activity is an important part of the environmental mechanisms leading to increased sediment fluxes in wetter (as a consequence of animal-triggered excavation and rainfall-triggered erosion) and drier (as a consequence of animal-triggered excavation) regions (Fig. 11).

https://doi.org/10.5194/esurf-2021-104
Preprint. Discussion started: 11 January 2022
© Author(s) 2022. CC BY 4.0 License.
Earth Surface Dynamics Discussions

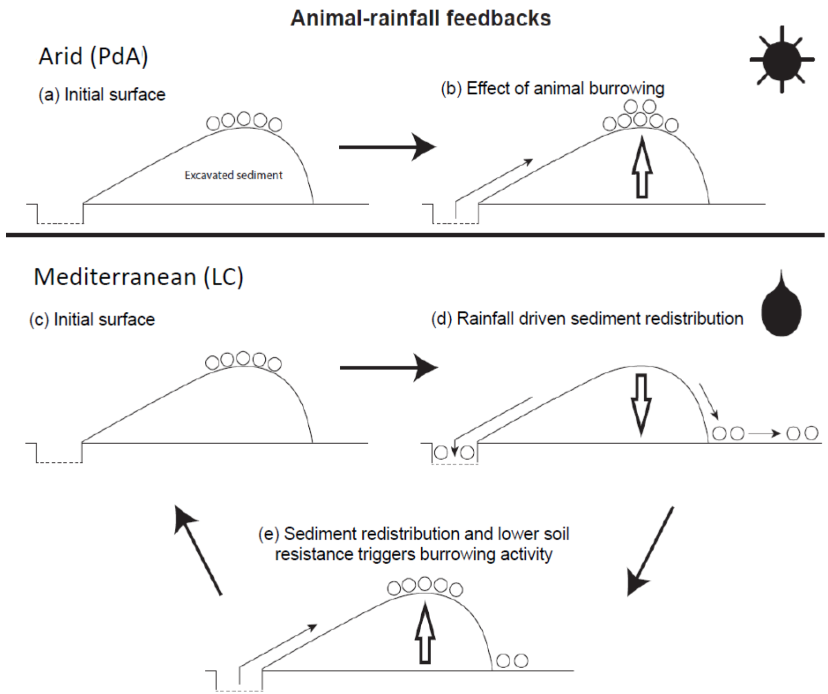

Figure 11. Scheme of the animal-driven and rainfall-driven sediment redistribution processes in both climate zones: (**a**) Describes the initial surface of the burrow before a start of a redistribution process and (**b**) the animal excavation process in the arid zone. Here, due to sporadically occurring rainfall events, sediment redistribution is mostly controlled by the animal burrowing activity; (**c**) Describes the initial burrow surface in the mediterranean climate zone, (**d**) the process of sediment redistribution during a rainfall event and (**e**) the following animal burrowing activity. The burrowing is triggered by decreased soil resistance due to the increased soil moisture after rainfall as well as by sediment accumulation within the burrow's entrance. The burrowing activity leads to a new supply of sediment being excavated to the surface. In the mediterranean climate zone, the sediment redistribution is controlled by both animal burrowing activity and rainfall. The alternating excavation and erosion process ultimately lead to an increase in redistribution rates.

Magnitudes of sediment volume redistributed within areas affected by burrowing animals similar to our results were previously obtained solely in studies applying rainfall simulator. These studies estimated an increase in the volume of sediment redistributed during rainfall events, measured in the areas affected by burrowing animals when compared to not affected areas, to be between 205% and 473% (Li et al., 2018; Chen et al., 2021), Table A6). However, a rainfall simulator can only provide data on surface processes within a plot of a few m^2 in size and under ideal laboratory conditions while ignoring the uphill microtopography, vegetation cover and distribution (Iserloh et al., 2013) which were shown to reduce erosion rates. More importantly, the rainfall intensity on hillslopes decreases with (i) the angle of incidence of the rain, (ii) the inclination of the surface and iii) the relative orientation of the sloping surface to the rain vector (Sharon, 1980). When simulating a rainfall event with the same rainfall volume as in the field, the rain is induced directly over the treated surface and has thus a higher velocity which leads to an increased splash erosion than under natural conditions (Iserloh

https://doi.org/10.5194/esurf-2021-104
Preprint. Discussion started: 11 January 2022
© Author(s) 2022. CC BY 4.0 License.

et al., 2013). We thus propose that the rainfall experiments overestimate the erosion rate while the correct erosion rate can be measured solely under field conditions.

Cumulative sediment redistribution within burrow roof, mound and entrance was, on average, 28% lower than cumulative sediment redistribution only within the mound and the burrow roof (Fig. 9 and A4). These results suggest that 28% of the eroded sediment from animal mounds and burrow roofs is re-accumulated within the burrow entrance during rainfall-runoff events, and the remaining 62% is incorporated into overall hillslope sediment flux. Our numbers contrast with previous studies, which quantified that about 58% of the sediment excavated by animals will accumulate back in the burrow entrance and only 42% is incorporated to downhill sediment flux (Andersen, 1987; Reichman and Seabloom, 2002). Hence, our results indicate not only higher redistribution rates within areas affected by the burrowing animals but also point to much higher supply of sediment to the downhill sediment flux as previously thought.

On the hillslope scale, the contrast between our estimated volume of redistributed sediment during rainfall events within areas affected by burrowing animals (from –0.67 until –1.18 cm^3 cm^{-2} $year^{-1}$) and the previous studies was even higher than on the burrow scale (from –0.183 until –1.56 cm^3 cm^{-2} $year^{-1}$, (Imeson and Kwaad, 1976; Li et al., 2018), Table A7). This was well pronounced when estimating the hillslope-wide volume of the sediment excavated by the animals (from 0.18 cm^3 cm^{-2} $year^{-1}$ until 0.67 cm^3 cm^{-2} $year^{-1}$ according to our study, and from 0.05 cm^3 cm^{-2} $year^{-1}$ until 0.49 cm^3 cm^{-2} $year^{-1}$ according to previous studies, (Black and Montgomery, 1991; Hall et al., 1999), Table A8). The previous studies estimated the area-wide excavated soil volume solely once or twice a year. We propose that these measurements only describe the current burrow distribution, however, cannot consider the continuous excavation and erosion dynamics.

Our study offers new insights previously undescribed in literature. Our cost-effective ToF device provides data on surface changes in a high spatio-temporal resolution. The high temporal resolution could unravel ongoing low magnitude but frequent excavation and erosion processes. High spatial resolution enabled us to estimate the exact volume of sediment fluxes from the burrows downhill. Our results indicate that the contribution of burrowing animals on the burrow as well as on the hillslope scale was much higher than previously assumed. In our future research, we intend to include our findings into long-term soil erosion models that rely on soil processes but do not yet include animal-induced surface processes on microtopographical scales in their algorithms.

6. Conclusion

Our study provides new insights on the impacts of burrowing animals on hillslope sediment fluxes. The continuous high-resolution monitoring enables to study the surface processes in detail and the high temporal data availability revealed higher redistribution rates within areas affected by burrowing animals than previously assumed. We discovered an alteration between sediment excavation by the animal and sediment erosion during rainfall events which unveil a continuous sediment contribution of burrowing animals to hillslope sediment flux. Although we concentrated on the impacts of burrowing animals on sediment redistribution, the applicability of the cameras is not limited to our research topic. Other possible applications could, for example, be a study of surface roughness, impacts of dead wood on erosion, biomass changes throughout the year or decomposition processes.

Funding: This study was funded by the German Research Foundation, DFG [grant numbers BE1780/52-1, LA3521/1-1, FA 925/12-1, BR 1293-18-1], and is part of the DFG Priority Programme

© Author(s) 2022. CC BY 4.0 License.

SPP 1803: EarthShape: Earth Surface Shaping by Biota, sub-project “Effects of bioturbation on rates of vertical and horizontal sediment and nutrient fluxes”.

Institutional Review Board Statement: Not applicable.

Informed Consent Statement: Not applicable.

Acknowledgments: We thank CONAF for the kind support provided during our field campaign.

Competing interests: There is no conflict of interest.

Author contribution: JB, AL and SA planned the campaign; PG and SA performed the measurements; PG analysed the data and wrote the manuscript draft; AL, JB, NF, RB, KÜ, LP, CR, DK and PP reviewed and edited the manuscript.

Code/Data availability: Code and all raw data can be provided by the corresponding author upon request.

Appendices

Table A1. List of abbreviations

α [°]	**Tilt angle of the camera**
b [°]	Surface inclination
Ω	Threshold value for the scan scattering error
A	Affected area
Affected area	Area directly affected by the burrowing animal
Area$_{burrow}$	mean in the field measured size of the burrows which are monitored
Area	total surface area monitored by the camera
BD	Bulk density
c [m/s]	Speed of light
D	Distance from the camera to the object
Dens$_{burrow}$	Burrow density
DSM	Digital surface model
DSM$_{after}$	DSM calculated from the scan taken after the extraction
DSM$_{before}$	DSM calculated from the scan taken before the extraction
Entrance	entrance to the animal burrow
g [-]	ratio [-] of the reflected photons to all photons
LC	National Park LC
LC-NL	Camera in LC on the lower north-facing hillslope
LC-NU	Camera in LC on the upper north-facing hillslope
LC-SL	Camera in LC on the lower south-facing hillslope
LC-SU	Camera in LC on the upper south-facing hillslope
MAE	Mean absolute error
MAP [°]	Mean annual precipitation
m.a.s.l.	Meters above sea level
MAT	Mean annual temperature
mClay [%]	Mean content of clay
mean$_{z\text{-}coordinate}$	Mean value of the z-coordinates

Mound	the sediment excavated by the animal while digging the burrow
mSand [%]	Mean content of sand
mSilt [%]	Mean content of silt
N	Number of scans
N	Not affected area
Not affected area	Area not directly affected by the burrowing animal
PdA	National Park Pan de Azúcar
PdA-NL	Camera in PdA on the lower north-facing hillslope
PdA-NU	Camera in PdA on the upper north-facing hillslope
PdA-SL	Camera in PdA on the lower south-facing hillslope
PdA-SU	Camera in PdA on the upper south-facing hillslope
Res	resolution
Roof	sediment pushed aside and uphill the entrance during burrow creation
S_a	scan after the rainfall event
S_b	scan before the rainfall event
SBC	Single board computer
$sd_{z\text{-coordinate}}$	standard deviation of the z-coordinates
SSH	Secure shell
t [s]	Overall time of camera illumination
TOC [%]	Total organic carbon
ToF	Time-of-Flight
$Vol_{affected}$	volume of redistributed sediment within affected area
$Vol_{detected}$	volume of the extracted sediment as detected by the camera
Vol_{add}	difference in redistributed sediment volume between affected and not affected areas
Vol_{exc}	Volume of the sediment excavated by the animal
$Vol_{hillslope\text{-}wide}$	Hillslope-wide volume of redistributed sediment
$Vol_{measured}$	volume of the extracted sediment measured by the measuring cup
$Vol_{per\ burrow}$	Volume of redistributed sediment per burrow
$Vol_{per\ pixel}$	Volume of redistributed sediment per pixel
$Vol_{redistributed}$	volume of the calculated redistributed sediment
$Vol_{not\ affected}$	volume of redistributed sediment within not affected area
y_i	distance of the point to the point of origin at the camera nadir
z_{cor}	Corrected z-coordinate
z_{uncor}	Uncorrected z-coordinate

Table A2. Number of usable scans for each camera

Camera	Latitude	Longitude	Number of scans	Percentage of usable scans taken at 1am / 5am / 8am / 10pm	Time period
PdA-NU	-25.98131	-70.6166	238	29 / 27 / 20 / 24	18.3.-18.9.

https://doi.org/10.5194/esurf-2021-104
Preprint. Discussion started: 11 January 2022
© Author(s) 2022. CC BY 4.0 License.

PdA-NL	-25.98277	-70.61278	52	24 / 0 / 40 / 36	27.3.-31.5
PdA-SU	-25.97477	-70.61641	351	30 / 26 / 32 / 11	16.3.-19.9.
PdA-SL	-25.97177	-70.61409	167	48 / 38 / 7 / 8	16.3.-19.9.
LC-NU	-32.95230	-71.06231	215	37 / 20 / 8 / 33	9.3.-9.9.
LC-NL	-32.93928	-71.08613	3	-	6.3.-12.9
LC-SU	-32.93078	-71.09066	160	22 / 28 / 26 / 25	28.3.-22.5
LC-SL	-32.93110	-71.08987	167	27 / 25 / 22 / 26	16.3.-19.9.

Table A3. Summary of the volume of redistributed sediment, according to area and disturbance type. Vol$_{exc}$ describes volume of the sediment excavated by the animals. Vol$_{affected}$ describes volume of the sediment redistributed during rainfall events within affected areas. Vol$_{add}$ describes the difference in redistributed sediment volume within affected and not affected area during rainfall.

Disturbance	**Area**	**PdA**	**LC**
Vol$_{exc}$	Affected area	16.41 cm^3 cm^{-2} year^{-1}	14.62 cm^3 cm^{-2} year^{-1}
	Per burrow	1498.66 cm^3 burrow^{-1} year^{-1}	1226.61 cm^3 burrow^{-1} year^{-1}
	Hillslope-wide	0.18 m^3 ha^{-1} year^{-1}	0.67 m^3 ha^{-1} year^{-1}
Vol$_{affected}$	Affected area	-1.97 cm^3 cm^{-2} year^{-1}	-10.44 cm^3 cm^{-2} year^{-1}
	Per burrow	-126.36 cm^3 burrow^{-1} year^{-1}	-876.38 cm^3 burrow^{-1} year^{-1}
	Hillslope-wide	-0.05 m^3 ha^{-1} year^{-1}	-0.48 m^3 ha^{-1} year^{-1}
Vol$_{add}$	Affected area	-1.18 cm^3 cm $^{-2}$ year^{-1}	-7.37 cm^3 cm^{-2} year^{-1}
	Per burrow	-48.36 cm^3 burrow^{-1} year^{-1}	-619.2 cm^3 burrow^{-1} year^{-1}
	Hillslope-wide	-0.02 m^3 ha^{-1} year^{-1}	-0.34 m^3 ha^{-1} year^{-1}

Table A4. Summary of the mass of redistributed sediment in Pan de Azúcar, according to area and disturbance type. Vol$_{exc}$ describes volume of the sediment excavated by the animals. Vol$_{affected}$ describes volume of the sediment redistributed during rainfall events within affected areas. Vol$_{add}$ describes the difference in redistributed sediment volume within affected and not affected area during rainfall.

Disturbance	**Area**	**PdA**	**LC**
Vol$_{exc}$	Affected area	20.18 g cm^{-2} year^{-1}	13.44 g cm^{-2} year^{-1}
	Per burrow	1843.35 g burrow^{-1} year^{-1}	1127.66 g burrow^{-1} year^{-1}
	Hillslope-wide	246.17 kg ha^{-1} year^{-1}	611.66 kg ha^{-1} year^{-1}
Vol$_{affected}$	Affected area	-1.73 g cm^{-2} year^{-1}	-9.6 g cm^{-2} year^{-1}
	Per burrow	-155.42 g burrow^{-1} year^{-1}	-806.26 g burrow^{-1} year^{-1}
	Hillslope-wide	-56.23 kg ha^{-1} year^{-1}	-436.97 kg ha^{-1} year^{-1}
Vol$_{add}$	Affected area	-1.45 g cm^{-2} year^{-1}	-6.79 g cm^{-2} year^{-1}

https://doi.org/10.5194/esurf-2021-104
Preprint. Discussion started: 11 January 2022
© Author(s) 2022. CC BY 4.0 License.

	Per burrow	-1.8 g $burrow^{-1}$ $year^{-1}$	-569.65 g $burrow^{-1}$ $year^{-1}$
	Hillslope-wide	-16.29 kg ha^{-1} $year^{-1}$	-308.57 kg ha^{-1} $year^{-1}$

Table A5. Review of studies which used laser scanners for the estimation of surface processes.

Reference	**R^2**	**Error**	**Horizontal point spacing**	**Points per cm^{-2}**	**Model**	**Price**
Our results	0.77	0.15 cm	0.32 cm	8.5	Texas Instruments OPT3101	900 $
(Eitel et al., 2011)	0.23-0.86	0.07 cm	NA	25	Leica ScanStation 2	102 375 $
(Eltner et al., 2013)	NA	0.4 cm	NA	6.4	Riegl LMS-Z420i	16 795
(Kaiser et al., 2014)	NA	NA	0.57 cm	NA	Riegl LMS-Z420i	16 795
(Longoni et al., 2016)	NA	NA	NA	1	Riegl LMS-Z420i	16 795
(Morris et al., 2011)	NA	0.5 cm	NA	NA	Maptek I-Site 4400LR	240 000
(Nasermoaddeli and Pasche, 2008)	NA	0.2 cm	0.25 cm	NA	Leica Cyrax HDS 2500	4500 $
(Thomsen et al., 2015)	NA	NA	0.4 cm	NA	Leica ScanStation 2	102 375 $

Table A6. Review of studies which estimated the sediment redistribution in areas affected and not affected areas and the proposed impact.

Reference	**Climate**	**Animals**	**Method**	**Monitoring period**	**Frequency**	**Affected areas**	**Not affected areas**	**impact**
Our results	arid	vertebrates	scanning	7 months	Daily	1.97 cm^3 cm^{-2} $year^{-1}$	1.39 cm^3 cm^{-2} $year^{-1}$	+40 %
Our results	mediterranean	vertebrates	scanning	7 months	daily	10.44 cm^3 cm^{-2} $year^{-1}$	1.39 cm^3 cm^{-2} $year^{-1}$	+338 %
(Imeson and Kwaad, 1976)	continental	rodents	erosion pins	15 months	monthly	20 mm		NA

https://doi.org/10.5194/esurf-2021-104
Preprint. Discussion started: 11 January 2022
© Author(s) 2022. CC BY 4.0 License.

(Imeson and Kwaad, 1976)	continental	rodents	splash boards	15 months	monthly	91.75g $24.49\ cm^{-2}$ = $3.75\ cm^3\ cm^{-2}$	94g	-3%
(Imeson and Kwaad, 1976)	continental	rodents	rainfall simulation (7.5 cm / hour intensity)	One-time measurement	NA	0.2 g – 0.73 g	0.009 g – 0.23 g	+208 %
(Imeson, 1977)	continental	vertebrates	rainfall simulation	One-time measurement	NA	0.18-0.3 100 $J^{-1}\ m^{-2}$ rain	0.146 100 $J^{-1}\ m^{-2}$ rain	+123 %
(Hazelhoff et al., 1981)	continental	earthworms	splash traps	12 months	monthly	NA	NA	+180 %
(Black and Montgomery, 1991)	arid	pocket gopher	erosion pins	10 months	2 months	NA	NA	+125 %
(Hakonson, 1999)	temperate	pocket gophers	rainfall simulator (60 mm / hour)	2 years	2 – 3 weeks	2.4 – 8.7 mg ha^{-1}	4.4 – 15 mg ha^{-1}	-43%
(Li et al., 2018)	temperate	mole crickets	rainfall simulation (36 mm / hour)	One time measurement	15 measurements	22.1 g 115 cm^{-2} = 5.2 $cm^3\ cm^{-2}$	5 g 123 cm^{-2} = 1.09 $cm^3\ cm^{-2}$	+473 %
(Li et al., 2018)	temperate	mole crickets	rainfall simulation (36 mm / hour)	One time measurement	15 measurements	35.3 g 220.5 cm^{-2} = 6.24 $cm^3\ cm^{-2}$	5 g 123 cm^{-2} = 1.09 $cm^3\ cm^{-2}$	+473 %
(Chen et al., 2021)	lab	chinese zocor	rainfall simulation (80 mm / hour)	One-time measurement	3 measurements	2,69 g cm^{-2} = 2.69 $cm^3\ cm^{-2}$	0,88 g cm^{-2} = 0.88 $cm^3\ cm^{-2}$	+205 %

https://doi.org/10.5194/esurf-2021-104
Preprint. Discussion started: 11 January 2022
© Author(s) 2022. CC BY 4.0 License.

Table A7. Review of studies which estimated the sediment redistribution in areas affected by burrowing animals, average burrow density as found in the literature and area-wide yearly contribution of burrowing animals to sediment redistribution.

Climate	Animals	Affected areas	Average burrow density	Average burrow size	Area-wide redistribution
Arid	vertebrates	1.97 cm^3 cm^{-2} $year^{-1}$	0-12 10 m^{-2} = 0-1.2 m^{-2} (Grigusova et al., 2021)	91.35 cm^2	1.18 cm^3 ha^{-2} $year^{-1}$
mediterranean	vertebrates	10.44 cm^3 cm^{-2} $year^{-1}$	6-12 10 m^{-2} = 0.6 – 1.2 m^{-2} (Grigusova et al., 2021)	84.36 cm^2	0.67 m^3 ha^{-1} $year^{-1}$
Continental	rodents	91.75g 24.49 cm^{-2} = 3.75 cm^3 cm^{-2} (Imeson and Kwaad, 1976)	14 625 m^{-2} = 0.02 m^{-2} (Pang and Guo, 2017)	24.49 cm^2 (Imeson and Kwaad, 1976)	0.183 m^3 ha^{-1} $year^{-1}$
Temperate	mole crickets	22.1 g 115 cm^{-2} = 5.2 cm^3 cm^{-2} (Li et al., 2018)	405 ha^{-1} (Castner and Fowler, 1984)	115 cm^2 (Li et al., 2018)	0.24 m^3 ha^{-1} $year^{-1}$
Temperate	mole crickets	35.3 g 220.5 cm^{-2} = 6.24 cm^3 cm^{-2} (Li et al., 2018)	405 ha^{-1} (Castner and Fowler, 1984)	220.5 cm^2 (Li et al., 2018)	0.56 m^3 ha^{-1} $year^{-1}$
Lab	chinese zocor	2,69 g cm^{-2} = 2.69 cm^3 cm^{-2} (Chen et al., 2021)	94.69 2500m^{-2} = 0.04 m^{-2} = 400 ha^{-1}	1256 cm^2	1.35 m^3 ha^{-1} $year^{-1}$

Table A8. Review of studies which estimated the volume of sediment excavated by burrowing animals.

	Climate	Animals	Method	Monitoring period	Frequency	volume of the excavated sediment
Our results	arid	vertebrates	scanning	7 months	daily	0.18 m^3 ha^{-1} $year^{-1}$
Our results	mediterranean	vertebrates	scanning	7 months	daily	0.67 m^3 ha^{-1} $year^{-1}$

https://doi.org/10.5194/esurf-2021-104
Preprint. Discussion started: 11 January 2022
© Author(s) 2022. CC BY 4.0 License.

(Black and Montgomery, 1991)	arid	porcupines	mound volume	3 years	yearly	0.2 m^3 ha^{-1} $year^{-1}$
(Black and Montgomery, 1991)	arid	isopods	mound volume	3 years	yearly	0.11 m^3 ha^{-1} $year^{-1}$
(Black and Montgomery, 1991)	arid	pocket gopher	mound volume	2 years	3 model runs	0.05 – 0.11 m^3 ha^{-1} $year^{-1}$
(Rutin, 1996)	subtropical	scorpions	mound volume	6 months	2-29 days	0.42 m^3 ha^{-1} $year^{-1}$
(Hall et al., 1999)	alpine	rodents	mound volume	1 year	yearly	0.02 m^3 ha^{-1} $year^{-1}$
(Hall et al., 1999)	alpine	bears	mound volume	1 year	yearly	0.49 m^3 ha^{-1} $year^{-1}$
(Yoo et al., 2005)	arid	pocket gopher	mound volume	1 year	One model run	0.1-0.2 m^3 ha^{-1} $year^{-1}$

https://doi.org/10.5194/esurf-2021-104
Preprint. Discussion started: 11 January 2022
© Author(s) 2022. CC BY 4.0 License.
Earth Surface Dynamics
Discussions

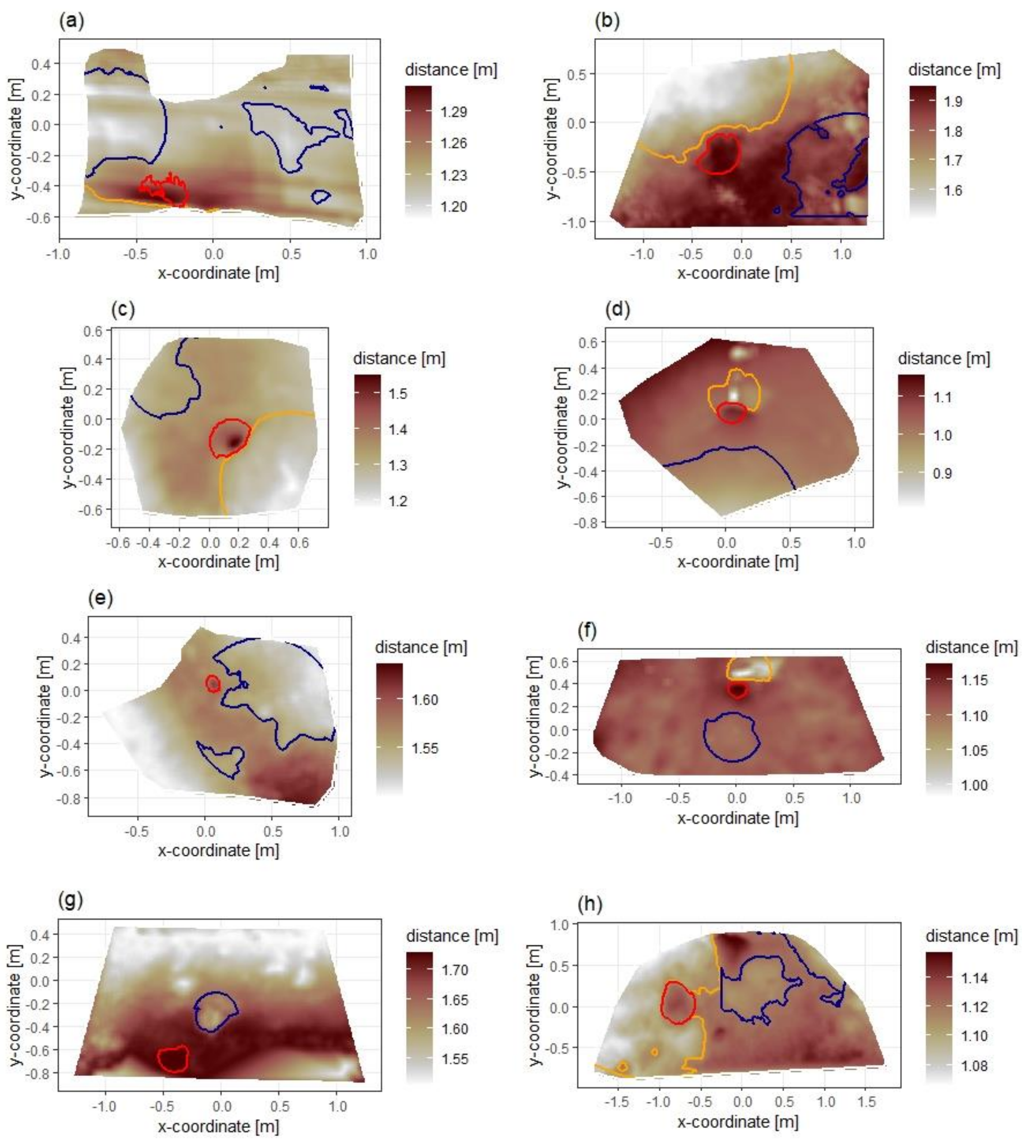

Figure A1. Delineation of the areas. The point of origin of the coordinate system is at the camera nadir. Depth is the distance between the surface and the camera. Red is the outline of the burrow entrance. Green is the outline of mound. Orange is the outline of burrow roof. Area which is not outlined is area not directly affected by the animal burrowing activity. Arrow indicates downhill direction of the hillslope. (a) LC-NU. (b) LC-NL (c) LC-SU. (d) LC-SL. (e) PdA-NU. (f) PdA-NL. (g) PdA-SU. (h) PdA-SL.

https://doi.org/10.5194/esurf-2021-104
Preprint. Discussion started: 11 January 2022
© Author(s) 2022. CC BY 4.0 License.
Earth Surface Dynamics
Discussions
Open Access

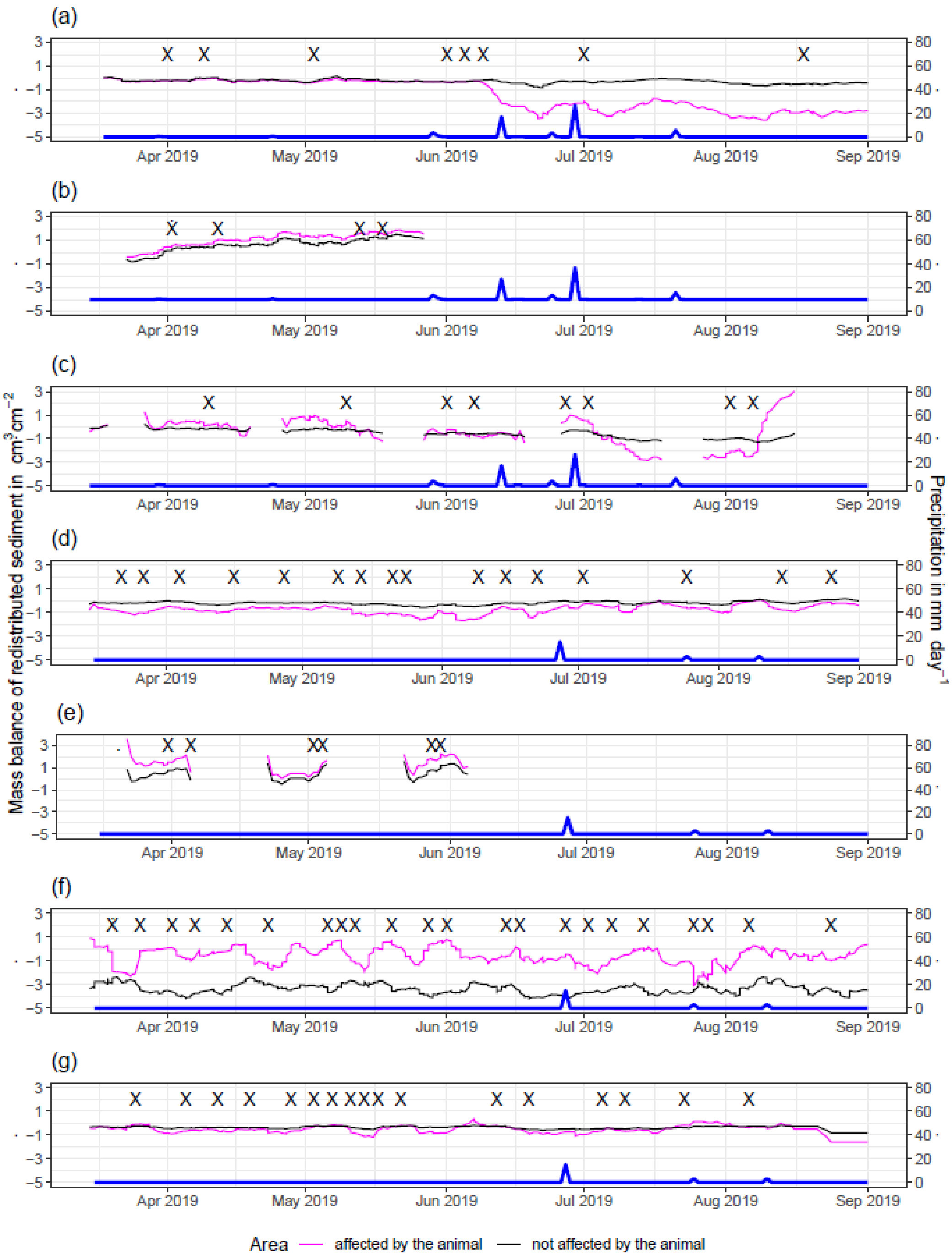

733
734 **Figure A2.** Sediment mass balance for the period of 7 months separately for areas affected and not affected
735 by burrowing animal as measured by the cameras. (a) LC-NU. (b) LC-SU. (c) LC-SL. (d) PdA-NU. (e) PdA-NL.
736 (f) PdA-SU. (g) PdA-SL. For abbreviations see Table A1.

https://doi.org/10.5194/esurf-2021-104
Preprint. Discussion started: 11 January 2022
© Author(s) 2022. CC BY 4.0 License.

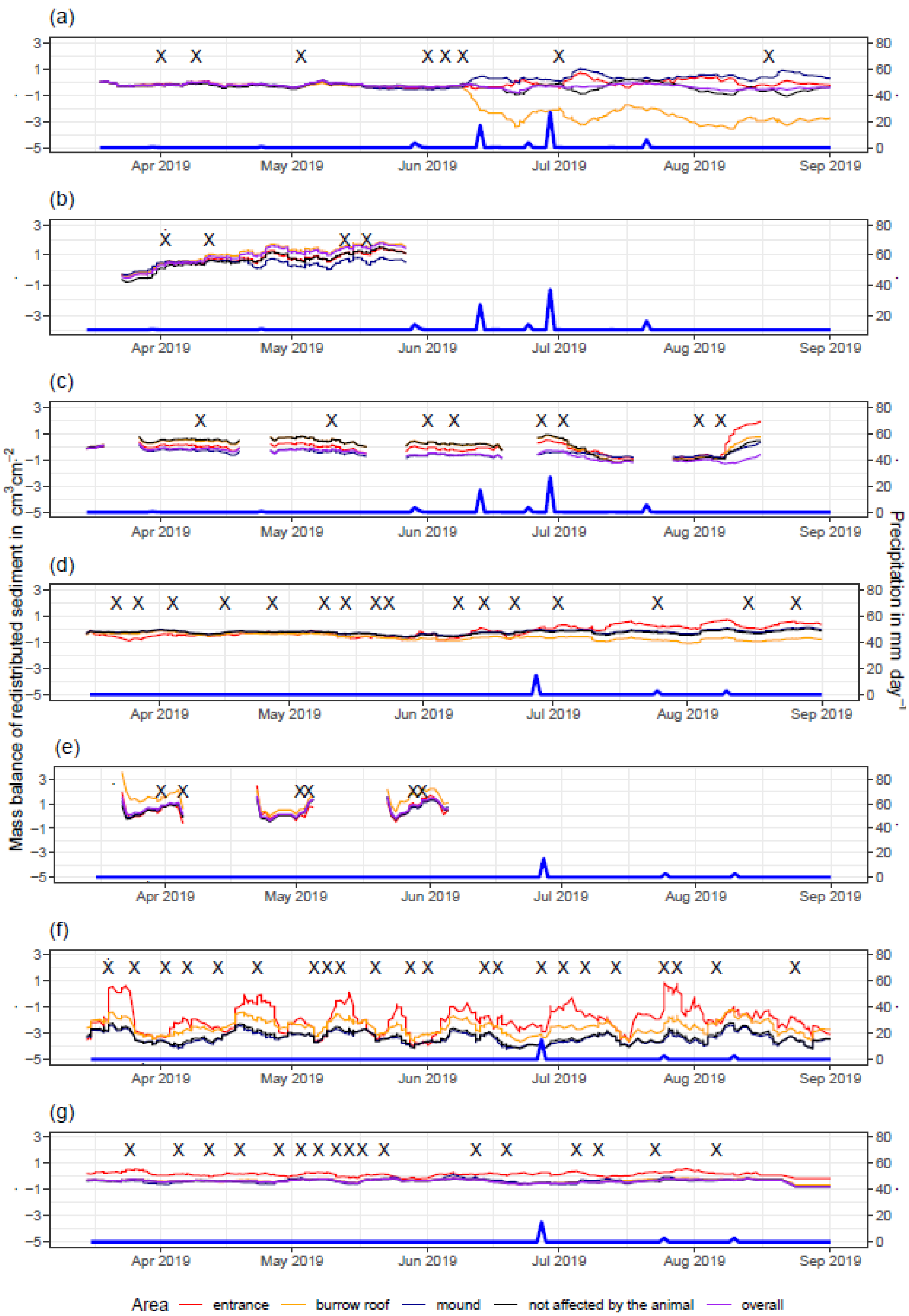

737

https://doi.org/10.5194/esurf-2021-104
Preprint. Discussion started: 11 January 2022
© Author(s) 2022. CC BY 4.0 License.

Earth Surface Dynamics
Discussions
Open Access
EGU

Figure A3. Sediment mass balance for the period of 7 months separately for all delineated areas as measured by the cameras. (a) LC-NU. (b) LC-SU. (c) LC-SL. (d) PdA-NU. (e) PdA-NL. (f) PdA-SU. (g) PdA-SL. For abbreviations see Table A1.

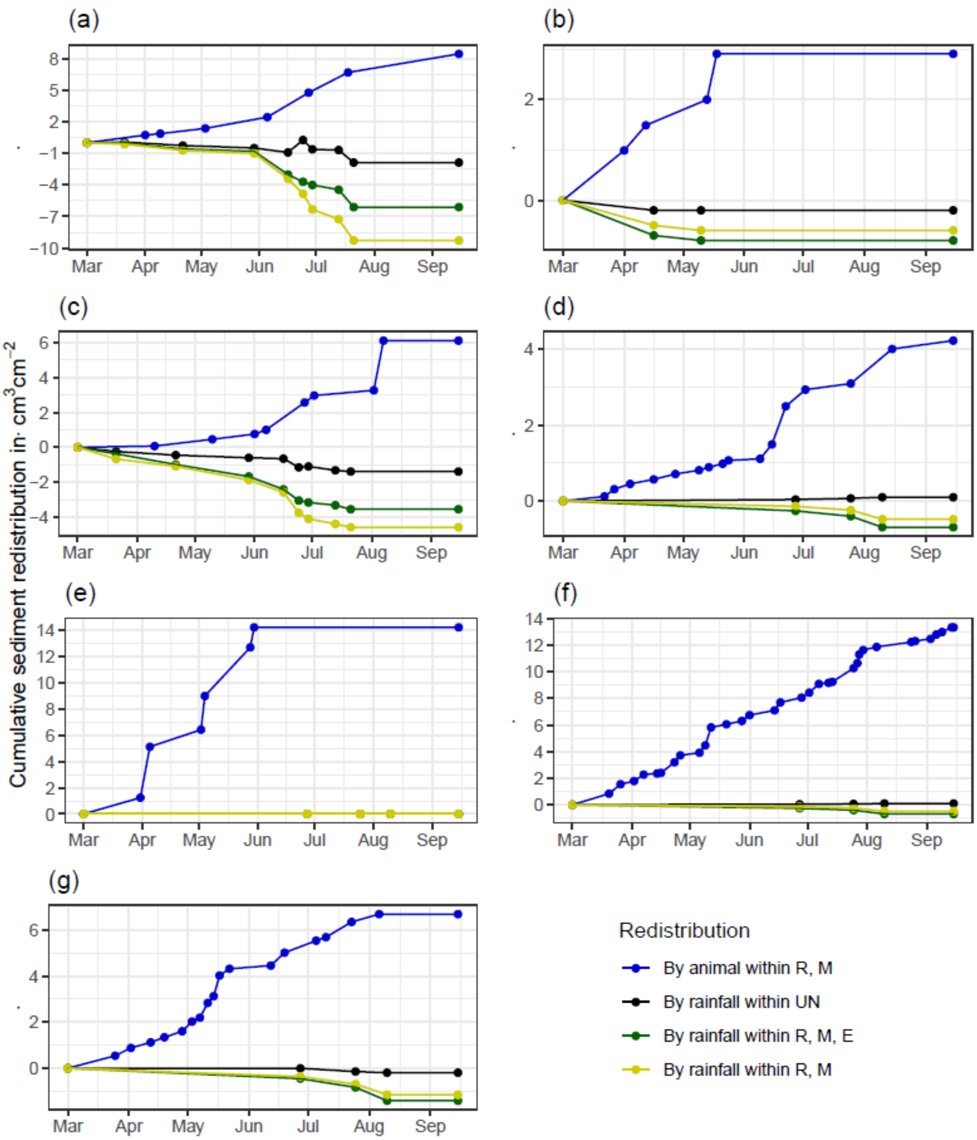

Figure A4. Cumulative volume of redistributed sediment for all cameras. Positive values indicate sediment accumulation. Negative values indicate sediment erosion. Whiskers are the median sediment redistribution. E is the burrow entrance. M is the mound. R is burrow roof. UN is area not directly affected by the animal burrowing activity. LC is mediterranean climate zone. PdA is arid climate zone. (a) LC-NU. (b) LC-SU. (c) LC-SL. (d) PdA-NU. (e) PdA-NL. (f) PdA-SU. (g) PdA-SL. For abbreviations see Table A1.

https://doi.org/10.5194/esurf-2021-104
Preprint. Discussion started: 11 January 2022
© Author(s) 2022. CC BY 4.0 License.
Earth Surface Dynamics
Discussions

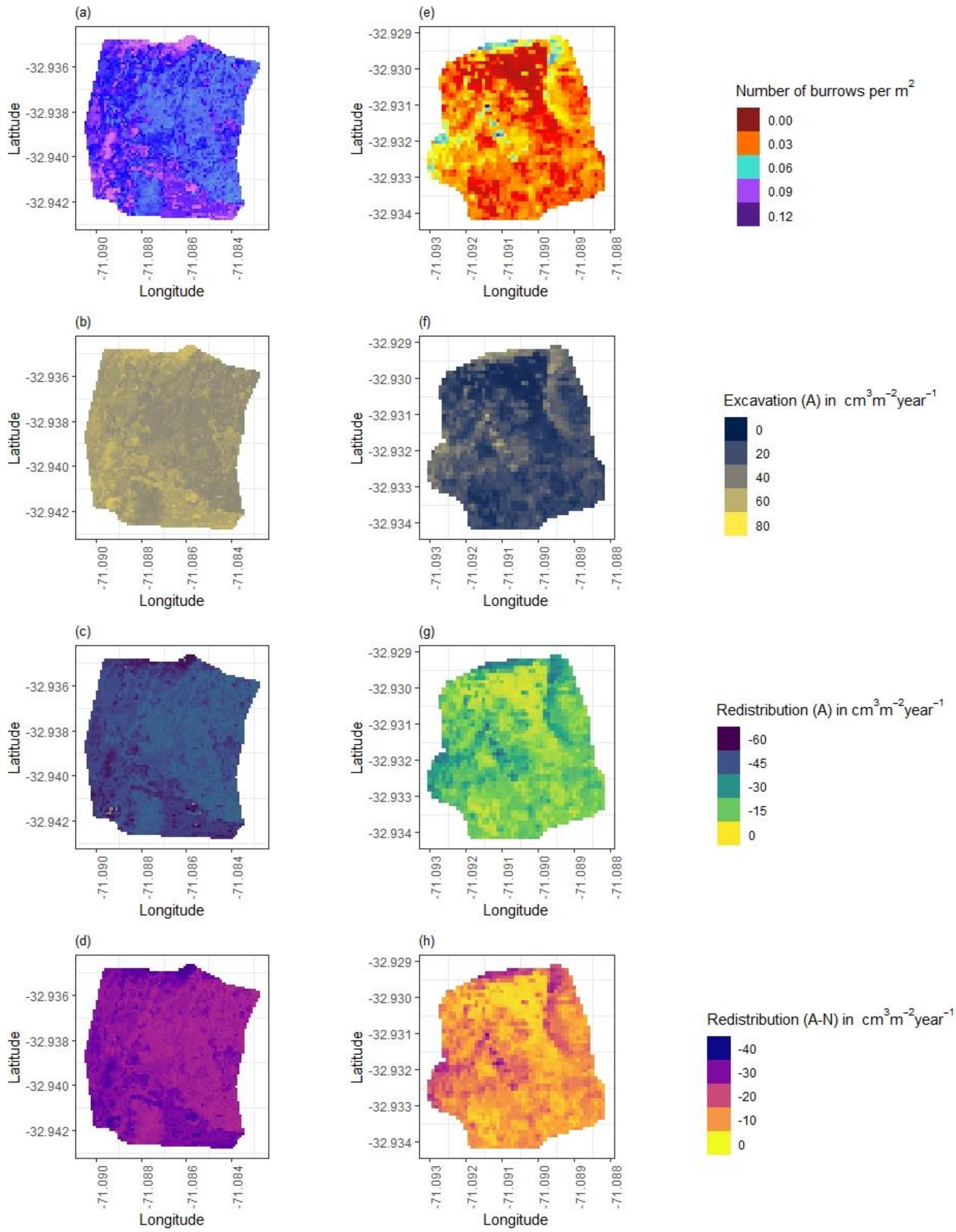

Figure A5. Hillslope-wide volume of redistributed sediment for a time period of one year in LC. (a-d) North-facing hillslope. (e-h) South-facing hillslope. (a) and (e) Density of burrows as estimated by Grigusova et al. 2021. (b) and (f) Volume of the sediment excavated by the animals. (c) and (g) Volume of the sediment redistributed during rainfall events within affected areas. (d) and (h) Volume of additionally redistributed sediment during rainfall events due to presence of the burrows. The values were calculated per burrow as stated in section 3.7 by subtracting the sediment volume redistributed within animal affected area from the

https://doi.org/10.5194/esurf-2021-104
Preprint. Discussion started: 11 January 2022
© Author(s) 2022. CC BY 4.0 License.

sediment volume redistributed within not affected area and then upscaled. A stays for affected area, N stays for not affected area by the burrowing animal.

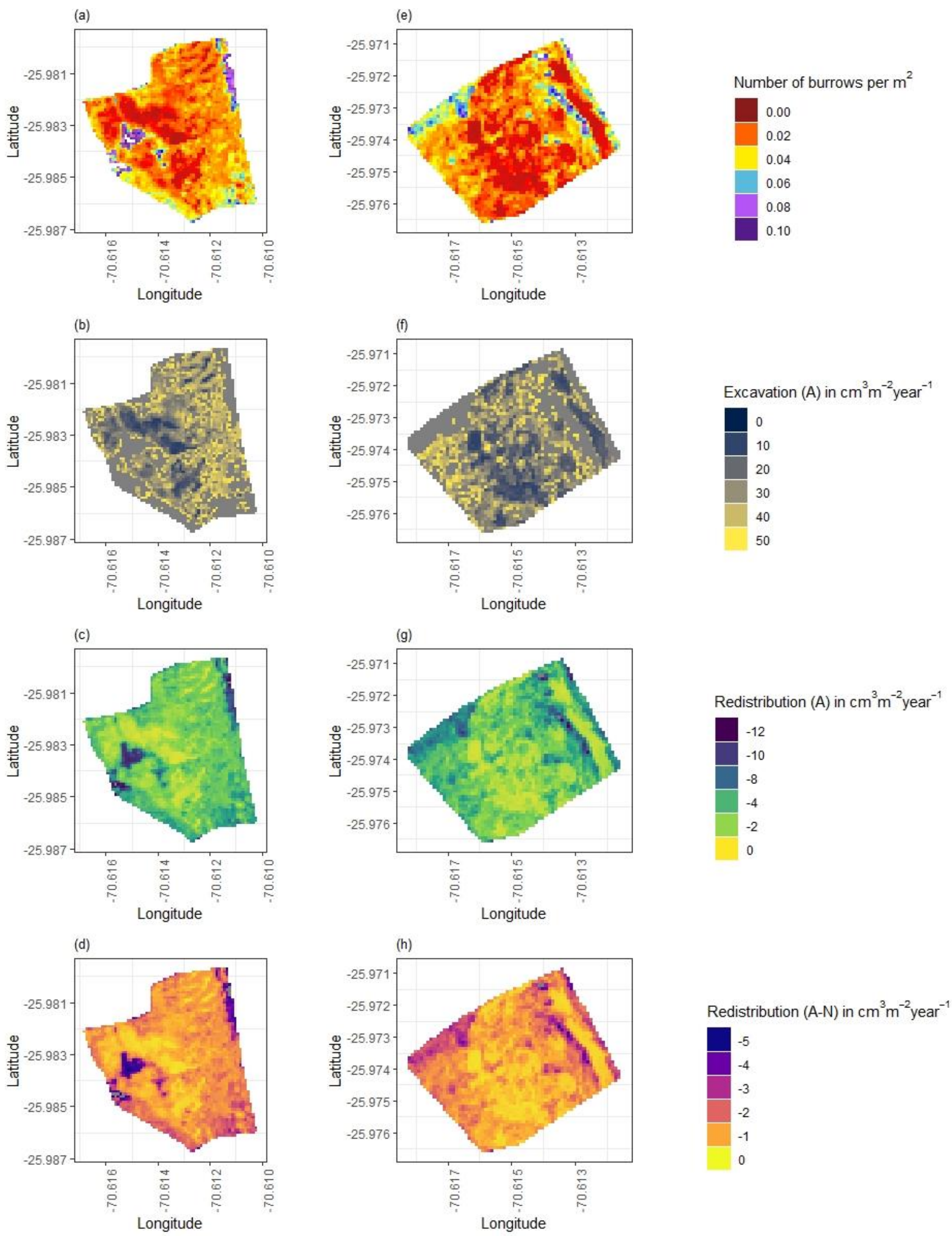

Figure A6. Hillslope-wide volume of redistributed sediment for a time period of one year in Pan de Azúcar. (a-d) North-facing hillslope. (e-h) South-facing hillslope. (a) and (e) Density of burrows as estimated by Grigusova et al. 2021. (b) and (f) Volume of the sediment excavated by the animals. (c) and (g) Volume of the sediment redistributed during rainfall events within affected areas. (d) and (h) Volume of additionally redistributed sediment during rainfall events due to presence of the burrows. The values were calculated per burrow as

https://doi.org/10.5194/esurf-2021-104
Preprint. Discussion started: 11 January 2022
© Author(s) 2022. CC BY 4.0 License.

stated in section 3.7 by subtracting the sediment volume redistributed within animal affected area from the sediment volume redistributed within not affected area and then upscaled. A stays for affected area, N stays for not affected area by the burrowing animal.

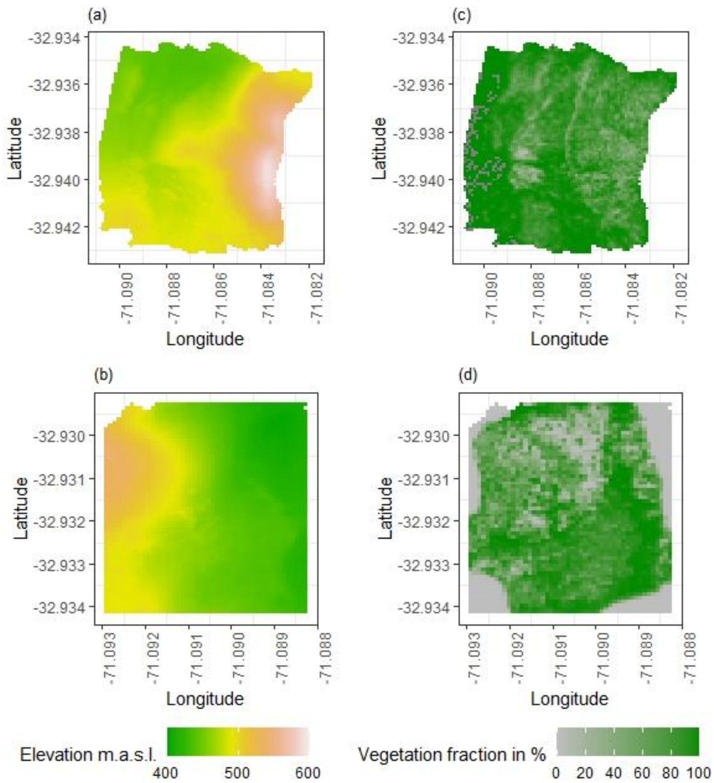

Figure A7. Digital surface model (a) and (b) and vegetation cover (c) and (d) of the hillslopes in LC. (a) and (c) North-facing hillslope. (b) and (d) South-facing hillslope. m.a.s.l stands for meters above sea level.

https://doi.org/10.5194/esurf-2021-104
Preprint. Discussion started: 11 January 2022
© Author(s) 2022. CC BY 4.0 License.

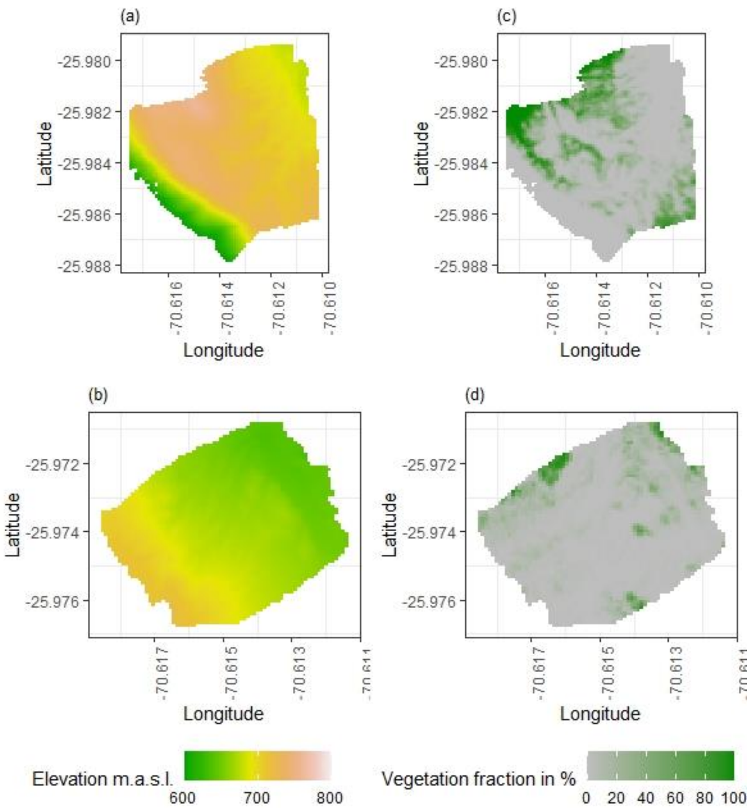

Figure A8. Digital surface model (a) and (b) and vegetation cover (c) and (d) of the hillslopes in Pan de Azúcar. (a) and (c) North-facing hillslope. (b) and (d) South-facing hillslope. m.a.s.l stands for meters above sea level.

https://doi.org/10.5194/esurf-2021-104
Preprint. Discussion started: 11 January 2022
© Author(s) 2022. CC BY 4.0 License.

References

Afana, A., Solé-Benet, A., and Pérez, J. L.: Determination of Soil Erosion Using Laser Scanners, last access: 22 December 2021.

Andersen, D. C.: Geomys Bursarius Burrowing Patterns: Influence of Season and Food Patch Structure, Ecology, 68, 1306–1318, doi:10.2307/1939215, 1987.

Ashcroft, M. B., Gollan, J. R., and Ramp, D.: Creating vegetation density profiles for a diverse range of ecological habitats using terrestrial laser scanning, Methods Ecol Evol, 5, 263–272, doi:10.1111/2041-210X.12157, 2014.

BANCROFT, W. J., HILL, D., and ROBERTS, J. D.: A new method for calculating volume of excavated burrows: the geomorphic impact of Wedge-Tailed Shearwater burrows on Rottnest Island, Funct Ecology, 18, 752–759, doi:10.1111/j.0269-8463.2004.00898.x, 2004.

Bernhard, N., Moskwa, L.-M., Schmidt, K., Oeser, R. A., Aburto, F., Bader, M. Y., Baumann, K., Blanckenburg, F. von, Boy, J., van den Brink, L., Brucker, E., Büdel, B., Canessa, R., Dippold, M. A., Ehlers, T. A., Fuentes, J. P., Godoy, R., Jung, P., Karsten, U., Köster, M., Kuzyakov, Y., Leinweber, P., Neidhardt, H., Matus, F., Mueller, C. W., Oelmann, Y., Oses, R., Osses, P., Paulino, L., Samolov, E., Schaller, M., Schmid, M., Spielvogel, S., Spohn, M., Stock, S., Stroncik, N., Tielbörger, K., Übernickel, K., Scholten, T., Seguel, O., Wagner, D., and Kühn, P.: Pedogenic and microbial interrelations to regional climate and local topography: New insights from a climate gradient (arid to humid) along the Coastal Cordillera of Chile, CATENA, 170, 335–355, doi:10.1016/j.catena.2018.06.018, 2018.

Black, T. A. and Montgomery, D. R.: Sediment transport by burrowing mammals, Marin County, California, Earth Surf. Process. Landforms, 16, 163–172, doi:10.1002/esp.3290160207, 1991.

Castner, J. L. and Fowler, H. G.: Distribution of Mole Crickets (Orthoptera: Gryllotalpidae: Scapteriscus) and the Mole Cricket Parasitoid Larra bicolor (Hymenoptera: Sphecidae) in Puerto Rico, The Florida Entomologist, 67, 481, doi:10.2307/3494730, 1984.

Chen, M., Ma, L., Shao, M.'a., Wei, X., Jia, Y., Sun, S., Zhang, Q., Li, T., Yang, X., and Gan, M.: Chinese zokor (Myospalax fontanierii) excavating activities lessen runoff but facilitate soil erosion – A simulation experiment, CATENA, 202, 105248, doi:10.1016/j.catena.2021.105248, 2021.

Coombes, M. A.: Biogeomorphology: diverse, integrative and useful, Earth Surf. Process. Landforms, 41, 2296–2300, doi:10.1002/esp.4055, 2016.

Eitel, J. U.H., Williams, C. J., Vierling, L. A., Al-Hamdan, O. Z., and Pierson, F. B.: Suitability of terrestrial laser scanning for studying surface roughness effects on concentrated flow erosion processes in rangelands, CATENA, 87, 398–407, doi:10.1016/j.catena.2011.07.009, 2011.

Eltner, A., Kaiser, A., Castillo, C., Rock, G., Neugirg, F., and Abellán, A.: Image-based surface reconstruction in geomorphometry – merits, limits and developments, Earth Surf. Dynam., 4, 359–389, doi:10.5194/esurf-4-359-2016, 2016a.

Eltner, A., Mulsow, C., and Maas, H.-G.: QUANTITATIVE MEASUREMENT OF SOIL EROSION FROM TLS AND UAV DATA, Int. Arch. Photogramm. Remote Sens. Spatial Inf. Sci., XL-1/W2, 119–124, doi:10.5194/isprsarchives-XL-1-W2-119-2013, 2013.

Eltner, A., Schneider, D., and Maas, H.-G.: INTEGRATED PROCESSING OF HIGH RESOLUTION

https://doi.org/10.5194/esurf-2021-104
Preprint. Discussion started: 11 January 2022
© Author(s) 2022. CC BY 4.0 License.

TOPOGRAPHIC DATA FOR SOIL EROSION ASSESSMENT CONSIDERING DATA ACQUISITION SCHEMES AND SURFACE PROPERTIES, Int. Arch. Photogramm. Remote Sens. Spatial Inf. Sci., XLI-B5, 813–819, doi:10.5194/isprsarchives-XLI-B5-813-2016, 2016b.

Gabet, E. J., Reichman, O. J., and Seabloom, E. W.: The Effects of Bioturbation on Soil Processes and Sediment Transport, Annu. Rev. Earth Planet. Sci., 31, 249–273, doi:10.1146/annurev.earth.31.100901.141314, 2003.

Grigusova, P., Larsen, A., Achilles, S., Klug, A., Fischer, R., Kraus, D., Übernickel, K., Paulino, L., Pliscoff, P., Brandl, R., Farwig, N., and Bendix, J.: Area-Wide Prediction of Vertebrate and Invertebrate Hole Density and Depth across a Climate Gradient in Chile Based on UAV and Machine Learning, Drones, 5, 86, doi:10.3390/drones5030086, 2021.

Hakonson, T. E.: The Effects of Pocket Gopher Burrowing on Water Balance and Erosion from Landfill Covers, J. environ. qual., 28, 659–665, doi:10.2134/jeq1999.00472425002800020033x, 1999.

Hall, K., Boelhouwers, J., and Driscoll, K.: Animals as Erosion Agents in the Alpine Zone: Some Data and Observations from Canada, Lesotho, and Tibet, Arctic, Antarctic, and Alpine Research, 31, 436–446, doi:10.1080/15230430.1999.12003328, 1999.

Hancock, G. and Lowry, J.: Quantifying the influence of rainfall, vegetation and animals on soil erosion and hillslope connectivity in the monsoonal tropics of northern Australia, Earth Surf. Process. Landforms, 46, 2110–2123, doi:10.1002/esp.5147, 2021.

Hänsel, P., Schindewolf, M., Eltner, A., Kaiser, A., and Schmidt, J.: Feasibility of High-Resolution Soil Erosion Measurements by Means of Rainfall Simulations and SfM Photogrammetry, Hydrology, 3, 38, doi:10.3390/hydrology3040038, 2016.

Hazelhoff, L., van Hoof, P., Imeson, A. C., and Kwaad, F. J. P. M.: The exposure of forest soil to erosion by earthworms, Earth Surf. Process. Landforms, 6, 235–250, doi:10.1002/esp.3290060305, 1981.

Herbst, M. and Bennett, N. C.: Burrow architecture and burrowing dynamics of the endangered Namaqua dune mole rat (Bathyergus janetta) (Rodentia: Bathyergidae), Journal of Zoology, 270, 420–428, doi:10.1111/j.1469-7998.2006.00151.x, 2006.

Horn, B.K.P.: Hill shading and the reflectance map, Proc. IEEE, 69, 14–47, doi:10.1109/PROC.1981.11918, 1981.

Imeson, A. C.: Splash erosion, animal activity and sediment supply in a small forested Luxembourg catchment, Earth Surf. Process. Landforms, 2, 153–160, doi:10.1002/esp.3290020207, 1977.

Imeson, A. C. and Kwaad, F. J. P. M.: Some Effects of Burrowing Animals on Slope Processes in the Luxembourg Ardennes, Geografiska Annaler: Series A, Physical Geography, 58, 317–328, doi:10.1080/04353676.1976.11879941, 1976.

Iserloh, T., Ries, J. B., Arnáez, J., Boix-Fayos, C., Butzen, V., Cerdà, A., Echeverría, M. T., Fernández-Gálvez, J., Fister, W., Geißler, C., Gómez, J. A., Gómez-Macpherson, H., Kuhn, N. J., Lázaro, R., León, F. J., Martínez-Mena, M., Martínez-Murillo, J. F., Marzen, M., Mingorance, M. D., Ortigosa, L., Peters, P., Regüés, D., Ruiz-Sinoga, J. D., Scholten, T., Seeger, M., Solé-Benet, A., Wengel, R., and Wirtz, S.: European small portable rainfall simulators: A comparison of rainfall characteristics, CATENA, 110, 100–112, doi:10.1016/j.catena.2013.05.013, 2013.

Jones, C. G., Gutiérrez, J. L., Byers, J. E., Crooks, J. A., Lambrinos, J. G., and Talley, T. S.: A framework for understanding physical ecosystem engineering by organisms, Oikos, 119, 1862–1869, doi:10.1111/j.1600-0706.2010.18782.x, 2010.

Kaiser, A., Neugirg, F., Rock, G., Müller, C., Haas, F., Ries, J., and Schmidt, J.: Small-Scale Surface Reconstruction and Volume Calculation of Soil Erosion in Complex Moroccan Gully Morphology Using Structure from Motion, Remote Sensing, 6, 7050–7080, doi:10.3390/rs6087050, 2014.

Kinlaw, A. and Grasmueck, M.: Evidence for and geomorphologic consequences of a reptilian ecosystem engineer: The burrowing cascade initiated by the Gopher Tortoise, Geomorphology, 157-158, 108–121, doi:10.1016/j.geomorph.2011.06.030, 2012.

Kukko, A. and Hyyppä, J.: Small-footprint Laser Scanning Simulator for System Validation, Error Assessment, and Algorithm Development, photogramm eng remote sensing, 75, 1177–1189, doi:10.14358/PERS.75.10.1177, 2009.

Larsen, A., Nardin, W., Lageweg, W. I., and Bätz, N.: Biogeomorphology, quo vadis? On processes, time, and space in biogeomorphology, Earth Surf. Process. Landforms, 46, 12–23, doi:10.1002/esp.5016, 2021.

Le Hir, P., Monbet, Y., and Orvain, F.: Sediment erodability in sediment transport modelling: Can we account for biota effects?, Continental Shelf Research, 27, 1116–1142, doi:10.1016/j.csr.2005.11.016, 2007.

Lehnert, L. W., Thies, B., Trachte, K., Achilles, S., Osses, P., Baumann, K., Bendix, J., Schmidt, J., Samolov, E., Jung, P., Leinweber, P., Karsten, U., and Büdel, B.: A Case Study on Fog/Low Stratus Occurrence at Las Lomitas, Atacama Desert (Chile) as a Water Source for Biological Soil Crusts, Aerosol Air Qual. Res., 18, 254–269, doi:10.4209/aaqr.2017.01.0021, 2018.

Li, G., Li, X., Li, J., Chen, W., Zhu, H., Zhao, J., and Hu, X.: Influences of Plateau Zokor Burrowing on Soil Erosion and Nutrient Loss in Alpine Meadows in the Yellow River Source Zone of West China, Water, 11, 2258, doi:10.3390/w11112258, 2019a.

Li, L.: Time-of-Flight Camera – An Introduction, Technical White Paper: https://www.ti.com/lit/wp/sloa190b/sloa190b.pdf, last access: 22 December 2021.

Li, T., Jia, Y., Shao, M.'a., and Shen, N.: Camponotus japonicus burrowing activities exacerbate soil erosion on bare slopes, Geoderma, 348, 158–167, doi:10.1016/j.geoderma.2019.04.035, 2019b.

Li, T., Shao, M.'a., Jia, Y., Jia, X., and Huang, L.: Small-scale observation on the effects of the burrowing activities of mole crickets on soil erosion and hydrologic processes, Agriculture, Ecosystems & Environment, 261, 136–143, doi:10.1016/j.agee.2018.04.010, 2018.

Li, T. C., Shao, M. A., Jia, Y. H., Jia, X. X., Huang, L. M., and Gan, M.: Small-scale observation on the effects of burrowing activities of ants on soil hydraulic processes, Eur J Soil Sci, 70, 236–244, doi:10.1111/ejss.12748, 2019c.

Longoni, L., Papini, M., Brambilla, D., Barazzetti, L., Roncoroni, F., Scaioni, M., and Ivanov, V.: Monitoring Riverbank Erosion in Mountain Catchments Using Terrestrial Laser Scanning, Remote Sensing, 8, 241, doi:10.3390/rs8030241, 2016.

Meysman, F. J. R., Boudreau, B. P., and Middelburg, J. J.: Relations between local, nonlocal, discrete and continuous models of bioturbation, Journal of Marine Research, 61, 391–410, doi:10.1357/002224003322201241, 2003.

Morris, R. H., Buckman, S., Connelly, P., Dragovich, D., Ostendorf, B., and and Bradstock, R. A.: The dirt on assessing post-fire erosion in the Mount Lofty Ranges: comparing methods: https://ro.uow.edu.au/scipapers/3474, last access: 22 December 2021.

Nasermoaddeli, M. B. and Pasche, E.: Application of terrestrial 3D scanner in quantification of the riverbank erosion and deposition: https://www.tuhh.de/t3resources/wb/Publikationen/MA-Veroeffentlichungen/nasermoaddeli/riverflow2008.pdf, last access: 22 December 2021.

https://doi.org/10.5194/esurf-2021-104
Preprint. Discussion started: 11 January 2022
© Author(s) 2022. CC BY 4.0 License.

Pang, X. P. and Guo, Z. G.: Plateau pika disturbances alter plant productivity and soil nutrients in alpine meadows of the Qinghai-Tibetan Plateau, China, Rangel. J., 39, 133, doi:10.1071/RJ16093, 2017.

Reichman, O. J. and Seabloom, E. W.: The role of pocket gophers as subterranean ecosystem engineers, Trends in Ecology & Evolution, 17, 44–49, doi:10.1016/S0169-5347(01)02329-1, 2002.

Richards, P. J. and Humphreys, G. S.: Burial and turbulent transport by bioturbation: a 27-year experiment in southeast Australia, Earth Surf. Process. Landforms, 21, n/a-n/a, doi:10.1002/esp.2007, 2010.

Ridd, P. V.: Flow Through Animal Burrows in Mangrove Creeks, Estuarine, Coastal and Shelf Science, 43, 617–625, doi:10.1006/ecss.1996.0091, 1996.

Romañach, S. S., Reichman, O. J., and Seabloom, E. W.: Seasonal influences on burrowing activity of a subterranean rodent, Thomomys bottae, Journal of Zoology, 266, 319–325, doi:10.1017/S0952836905006941, 2005.

Rutin, J.: The burrowing activity of scorpions (Scorpio maurus palmatus) and their potential contribution to the erosion of Hamra soils in Karkur, central Israel, Geomorphology, 15, 159–168, doi:10.1016/0169-555X(95)00120-T, 1996.

Sarbolandi, H., Plack, M., and Kolb, A.: Pulse Based Time-of-Flight Range Sensing, Sensors (Basel, Switzerland), 18, doi:10.3390/s18061679, 2018.

Schiffers, K., Teal, L. R., Travis, J. M. J., and Solan, M.: An open source simulation model for soil and sediment bioturbation, PloS one, 6, e28028, doi:10.1371/journal.pone.0028028, 2011.

Sharon, D.: The distribution of hydrologically effective rainfall incident on sloping ground, Journal of Hydrology, 46, 165–188, doi:10.1016/0022-1694(80)90041-4, 1980.

Thomsen, L. M., Baartman, J. E. M., Barneveld, R. J., Starkloff, T., and Stolte, J.: Soil surface roughness: comparing old and new measuring methods and application in a soil erosion model, SOIL, 1, 399–410, doi:10.5194/soil-1-399-2015, 2015.

Übernickel, K., Ehlers, T. A., Paulino, L., and Fuentes Espoz, J.-P.: Time series of meteorological stations on an elevational gradient in National Park La Campana, Chile, 2021a.

Übernickel, K., Pizarro-Araya, J., Bhagavathula, S., Paulino, L., and Ehlers, T. A.: Reviews and syntheses: Composition and characteristics of burrowing animals along a climate and ecological gradient, Chile, Biogeosciences, 18, 5573–5594, doi:10.5194/bg-18-5573-2021, 2021b.

Voiculescu, M., Ianăş, A.-N., and Germain, D.: Exploring the impact of snow vole (Chionomys nivalis) burrowing activity in the Făgăraș Mountains, Southern Carpathians (Romania): Geomorphic characteristics and sediment budget, CATENA, 181, 104070, doi:10.1016/j.catena.2019.05.016, 2019.

Wei, X., Li, S., Yang, P., and Cheng, H.: Soil erosion and vegetation succession in alpine Kobresia steppe meadow caused by plateau pika—A case study of Nagqu County, Tibet, Chin. Geograph.Sc., 17, 75–81, doi:10.1007/s11769-007-0075-0, 2007.

Wilkinson, M. T., Richards, P. J., and Humphreys, G. S.: Breaking ground: Pedological, geological, and ecological implications of soil bioturbation, Earth-Science Reviews, 97, 257–272, doi:10.1016/j.earscirev.2009.09.005, 2009.

Yair, A.: Short and long term effects of bioturbation on soil erosion, water resources and soil development in an arid environment, Geomorphology, 13, 87–99, doi:10.1016/0169-555X(95)00025-Z, 1995.

Yoo, K., Amundson, R., Heimsath, A. M., and Dietrich, W. E.: Process-based model linking pocket gopher (Thomomys bottae) activity to sediment transport and soil thickness, Earth Surf. Process. Landforms, 33, 917, doi:10.1130/G21831.1, 2005.